Università degli Studi di Padova

Dipartimento di Ingegneria Industriale

Corso di Laurea Magistrale in Ingegneria Aerospaziale

Alignment and characterization of HYPSOS

Relatore
Prof. Giampiero Naletto

Correlatori
Livio Agostini
Andrea Meneguzzo

Candidato
Emanuele Desiro'

Anno Accademico 2021-2022

A tutti coloro
che mi hanno supportato
in questi anni di studio

Abstract

The main objective of HYPSOS is to provide data about the spectrum and 3D stereovision environment reconstruction performed by a single instrument. In order to achieve this goal, it is fundamental that the instrument is aligned and characterized precisely. Milestones for the alignment and the characterization of the TMA telescope and the spectrometer will be introduced and discussed in this thesis. Both the components have been studied on the optical bench, and using laser beams.

Sommario

L'obiettivo principale di HYPSOS è fornire dati riguardanti lo spettro e la ricostruzione dell'ambiente 3D mediante stereovisione usando un unico strumento. Per raggiungere tale scopo è fondamentale che lo strumento sia correttamente allineato e caratterizzato. In questa tesi, verranno introdotti e affrontati i passaggi chiave che hanno permesso di raggiungere l'allineamento del telescopio TMA e dello spettrometro.
Nel primo capitolo verranno introdotti concetti chiave riguardanti la luce, i telescopi e gli spettrometri con particolare attenzione ai telescopi TMA e ai reticoli di diffrazione.
Nel secondo capitolo sarà introdotto HYPSOS e saranno fornite le specifiche tecniche dei vari componenti ottici e non che costituiscono lo strumento.
Nel terzo capitolo sarà presentato l'intero setup sperimentale utilizzato durante tutto lo studio e le tecniche per ottenere e verificarne l'allineamento.
Nel quarto capitolo sarà affrontato la caratterizzazione e l'allineamento dello spettrometro. Nello specifico, verrà descritta la caratterizzazione del sistema di lenti mediante il calcolo della posizione di fuoco e della relativa dimensione dello spot. Successivamente, verrà discusso l'allineamento del reticolo di diffrazione all'interno dello spettrometro. Con l'assemblaggio del detector e della fenditura, è stato possibile calcolare la curva spettrale e la FWHM degli spot. Durante l'analisi, uno studio qualitativo di eventuali straylight ha permesso di individuare e risolvere tale problema.
Nel quinto capitolo, verrà presentata la caratterizzazione degli specchi M1 e M3 del telescopio per verificarne la corretta costante conica. Successivamente, sarà discusso il metodo di allineamento dei prismi. Infine, verrà presentato l'allineamento degli specchi all'interno del telescopio e lo studio della MTF.
Nel sesto capitolo, un iniziale assemblaggio dello spettrometro sul telescopio sarà presentato per studiare una prima caratterizzazione dell'intero strumento.
Infine, nel settimo e ultimo capitolo, saranno riassunte le conclusioni con riferimenti ai risultati raccolti durante l'intero lavoro di tesi.

Contents

Listing of figures

Listing of tables

Listing of acronyms

BS . . . . . Beam Splitter

CTF . . . . . Contrast Transfer Function

DN . . . . . Digital Number

ESF . . . . . Edge Spread Function

FoV . . . . . Field of View

FM . . . . . Folding Mirror

FWHM . . . . . Full Width at Half Maximum

HYPSOS . . . . . HYPerspectral Stereo Observating System

LSF . . . . . Line Spread Function

NIST . . . . . National Institute of Standards and Technology

MTF . . . . . Modulation Transfer Function

TMA . . . . . Three Mirror Anastigmatic

SPP . . . . . Schimdt-Pechan Prism

1 Introduction

1.1 The concept of light

The visible light is the range of the electromagnetic radiation with a wavelength between $400\ nm$ and $750\ nm$. In modern physics, all the electromagnetic radiation can be modelled as a wave on both electric and magnetic field with a propagation velocity in vacuum around $c = 299\ 792\ 458\ m/s$. Due to this model, the main feature of electromagnetic radiation is the distance between two crests, or wavelength. Such characteristic allows to divide it in different categories, as shown in Figure 1.1:

- Radio waves [$\lambda > 30\ cm$] are primarily generated artificially through electrical oscillating circuits. It is vastly used in communication for television and radio broadcasts. The production, and the reception of such radiation requires large antennas. Due to the long wavelength, the frequency is low, and the energy is consequently low.

- Microwaves [$1\ mm < \lambda < 30\ cm$] are very important for many satellites because the atmosphere is transparent to them. As in the case of radio waves, to detect them antennas are required. In astronomy, they provide valuable information about stars and even the Big Bang.

- Infrared waves [$750\ nm < \lambda < 1\ mm$] are wavelengths typically connected with the heat because used to estimate the temperature of the objects with near room temperature. Other applications of the infrared radiations are communication, and meteorology studies.

- Visible light [$400\ nm < \lambda < 750\ nm$] is the range of the radiation visible with naked eye. Nowadays, there are many instruments used as light source, such as lasers, or to detect this radiation, as cameras.

- Ultraviolet rays [$6\ nm < \lambda < 400\ nm$] carry more energy than visible light and have shorter wavelengths. The main sources of ultraviolet radiation are the stars, for example the Sun.

- X-rays [$6\ pm < \lambda < 6\ nm$] are the radiation with high energy that can penetrate different materials. They are used to study internal components of engines or other machines in order to check for cracks or damaged parts.

- Gamma rays [$\lambda < 6\ nm$] are the radiation with extremely high energy. In astronomy, gamma rays are generated by galaxies, and other celestial bodies as black holes or neutron stars.

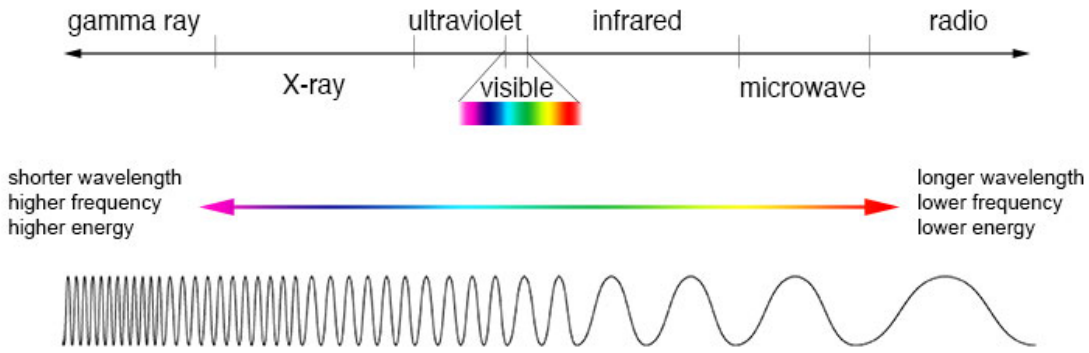

Figure 1.1: The electromagnetic spectrum

Electromagnetic radiation's physical definition is related to Maxwell's equations:

$$\begin{aligned} \nabla \cdot \mathbf{E} &= \frac{\rho}{\varepsilon_0} \\ \nabla \cdot \mathbf{B} &= 0 \\ \nabla \times \mathbf{E} &= -\frac{\partial \mathbf{B}}{\partial t} \\ \nabla \times \frac{\mathbf{B}}{\mu_\mathbf{0}} &= \varepsilon_0 \frac{\partial \mathbf{B}}{\partial t} + \mathbf{J} \end{aligned} \tag{1.1}$$

Where E and B are respectively the electrical and magnetic fields. These equations describe completely electromagnetic waves which travel at the speed of light, and they are the solutions

of this system of equations. The speed of light is also related to the electric constant ε_0 and the magnetic constant μ_0. It can be calculated as shown in the Equation 1.2.

$$c = 1/\sqrt{\varepsilon_0 \mu_0} \tag{1.2}$$

In optics, the equation set can be modified to the form shown in the Equation 1.3.

$$\nabla^2 \mathbf{E} - \mu_0 \varepsilon_0 \frac{\partial^2 \mathbf{E}}{\partial t^2} = \mu_0 \frac{\partial \mathbf{J}_{free}}{\partial t} + \mu_0 \frac{\partial^2 \mathbf{P}}{\partial t^2} - \frac{1}{\varepsilon_0} \nabla (\nabla \cdot \mathbf{P}) \tag{1.3}$$

The first term on the right side of the equation describes the reflection of light on metallic surfaces. The second one describes dipole oscillations, while the last term is useful for anisotropic materials as crystals. The terms on the left side describe light wave in vacuum when the right side is set to zero as shown in the Equation 1.4.

$$\nabla^2 \mathbf{E} - \mu_0 \varepsilon_0 \frac{\partial^2 \mathbf{E}}{\partial t^2} = 0 \tag{1.4}$$

To describe a light wave in a material, at least one of the terms on the right side is nonzero.

In many optics applications light as a wave can be replaced by a simpler description as a ray. With this representation it is possible to predict many information as the focal point position of an optical system, but it fails in the study of diffraction phenomena. Light as ray obeys to five laws of optics: rectilinear propagation in a homogeneous medium, invertibility of rays, independence of rays between each other, law of reflection and law of refraction. The first property is connected to the definition of ray as normal to the wavefront. The second one represents the property of rays to follow the same path from a starting point to an ending point, and from the ending point to the starting one. The third one is due to the fact that rays are lines, and they can be studied singularly without taking account of others. The law of reflection describes how rays are bounced after striking a surface. Parallel rays of light reaching an ideal and perfectly smooth surface are reflected remaining parallel. In particular, the reflected ray has the same angle of the incident ray respect to the surface's normal vector as shown in the Equation 1.5.

$$\theta_1 = \theta_2 \tag{1.5}$$

where:

θ_1 is the angle between the incident ray and the normal to the surface.

θ_2 is the angle between the reflected ray and the normal to the surface.

It is clear that a ray falling on a surface normally will be reflected along the same direction. In case the surface has micro-roughness, rays are reflected in many different directions losing the parallelism. In this condition the incident light is reflected as diffuse light.

The process of refraction is described by Snell's law in the Equation 1.6 and shown in Figure 1.2.

$$n_1 \sin\theta_1 = n_2 \sin\theta_2 \tag{1.6}$$

where:

n is the refractive index which is a function of the wavelength. This means that the same material refracts different wavelengths in different ways.

θ is the angle between the incident or refracted ray and the normal to the surface.

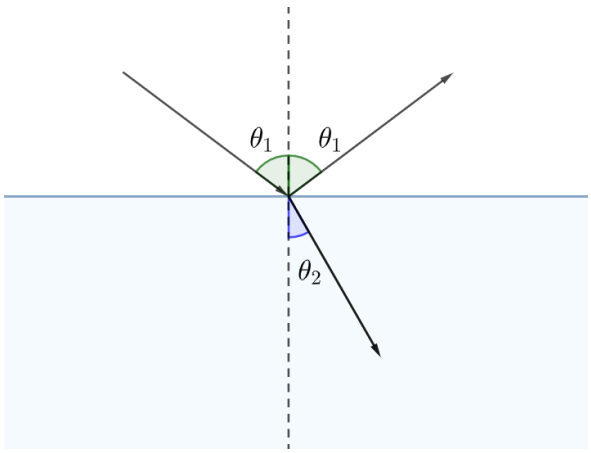

Figure 1.2: Reflection and refraction of a ray

In case the coming ray creates an angle with the normal close to 90 degrees, the refracted ray is close to the critical angle ϕ_c given by the Equation 1.7.

$$\sin\phi_c = \frac{n_1}{n_2} \tag{1.7}$$

Considering the principle of invertibility of rays, it is possible to determinate that a ray cannot be transmitted if $\theta_1 > \phi_c$. In this condition a total reflection takes place, and no ray is refracted but just reflected.

1.2 Introduction to telescopes

A telescope is an optical system formed by a combination of lenses and/or mirrors, and capable of providing information through the collection of light or electromagnetic radiation in general. Many telescope designs exist to be applied in different scientific fields or to obtain different advantages. Considering the design, telescopes are divided in three main categories: refractive telescopes, formed by lenses; reflecting telescopes, formed by mirrors; and catadioptric telescopes, formed by a combination of lenses and mirrors.
In general, telescopes are defined by different parameters, but the main ones are:

- Focal length: the distance between the telescope aperture and the focal point. It represents the path the light travels inside the telescope.
- Aperture: a parameter that represents the quantity of light collected by the telescope. Bigger apertures mean brighter images.
- Angular resolution: the ability of a telescope to resolve small details or objects. The minimal angle, that can be resolved by an instrument limited by diffraction, can be calculated with the Rayleigh criterion as shown in the Equation 1.8

$$\sin\theta_r = 1.22\,\frac{\lambda}{d} \tag{1.8}$$

where:

θ_r is the minimal resolvable angle.

λ is the wavelength of the incoming light.

d is the diameter of a circular aperture.

- Angular magnification: the ratio between the angle subtended by the image of an object seen by a telescope, and the angle subtended by the same object without the instrument. It can be calculated as shown in the Equation 1.9. A higher magnification can be obtained at the cost of a reduced observed FoV. This definition concerns only afocal telescopes.

$$M_A = \frac{f}{f_e} \tag{1.9}$$

where:

M_A is the angular magnification.

f is the focal length of the optical system.

f_e is the focal length of the eyepiece lens.

- Focal ratio: the ratio between the focal length and the aperture as show in the Equation 1.10. This parameter is also an index of the image's brightness between telescopes with equal other features.

$$f/\# = \frac{f}{d} \tag{1.10}$$

The images generated by telescopes are not perfect due to the fact that lenses and mirrors have imperfections. These defects in the image are called aberrations and are divided in monochromatic (Seidel aberrations) and chromatic ones. The five Seidel aberrations are:

- Coma: a point light source appears as a comet-shape.
- Distortion: the image is radially distorted as a barrel or pincushion.
- Astigmatism: a point light source appears along the through focus as oblong ellipse along the sagittal or tangential direction.
- Spherical aberration: collimated rays are focused on different position in relation to the distance between the considered ray and the optical axis of the instrument.
- Petzval field curvature: collimated rays with different angle respect to the optical axis are focused not on a flat surface but on a curved one.

Concerning the chromatic aberration, it is a defect in the image related with the wavelength of the observed radiation. Different wavelengths are focused on different positions of the focal plane (transverse chromatic aberration) or on different focal planes (longitudinal chromatic aberration).

1.2.1 Three Mirror Anastigmat telescopes

A Three-Mirror Anastigmatic telescope is a particular design with the purpose to minimize four aberrations: astigmatism, coma, spherical aberration, and Petzval field curvature. The typical TMA design is formed by a primary mirror that converges the light in a secondary mirror. The reflected light creates a secondary image before to reach the tertiary mirror, which creates the final image. A flat mirror is placed to form the image away from the telescope for a more convenient configuration. The described design is shown in the Figure 1.3

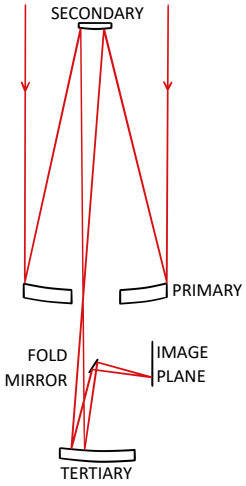

Figure 1.3: Design of a TMA

In another possible design of the TMA, a perforated mirror is required. In this case, the reflected light by the secondary mirror reaches the perforated mirror which redirects the rays to the tertiary mirror. Then, the light is reflected and converges to the image plane passing through the perforated mirror. The advantage of this design is a significant improvement of the baffling of the system. Concerning the stray light, the first described design requires at least one scattering process before the light can reach the final image, while in the second design just a single process is not enough.

Some advantages in the selection of a TMA telescope are smaller volume, a wide spectral range and the correction of the aberration described before. These features make the TMA telescope design more convenient in space missions.

1.3 Introduction to spectrometers

Spectrometers are optical instruments widely used to separate and study the spectrum of an object. Typically, a spectrometer is formed by an aperture that collects light from the source, an optical element which divides the wavelengths, and a detector which collects them. The spectral components are dispersed along different directions depending on the atomic elements of the studied object. For this reason, a correct calibration of the spectrometer is fundamental, and it can be performed using spectral lamps. Every spectral lamp corresponds to a specific element or a

combination of them, with well-known spectral components. Without any variation in the optical configuration, those wavelengths reach the detector in the same position along the spectral direction, which permits to calibrate the spectrometer.

The most fundamental component in a spectrometer is the optical element which provides the spectral dispersion. This element can be a prism or a diffraction grating, both are shown in Figure 1.4. The first collects the light which, traveling though the element, gets divided into its spectral components. This phenomenon is possible due to the angle of refraction, which depends on the refractive index, and which is function of the wavelength. While a diffraction grating uses a surface with grooves that provides the spectral diffraction of the light.

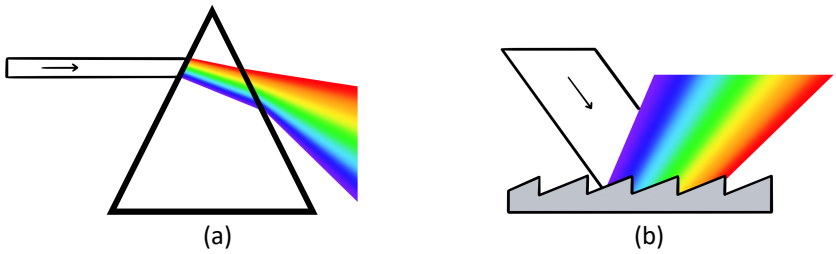

Figure 1.4: (a) Prism (b) Diffraction grating

Diffraction gratings divide the light in diffracted orders conventionally numbered from 0, both positive and negative. The zeroth order corresponds to the usual reflection of light without any spectral dispersion. The sign is positive or negative if the reflection beam is, respectively, on the same or opposite side of the incident ray respect to the 0th order, as show in the Figure 1.5.

Spectrometers can analyse both the absorption and emission spectrum. In case of a light source, such as a spectral lamp, the acquired spectrum is an emission one. This phenomenon is connected to the release of photons when an element is in an excited state. While in the process of studying an absorption spectrum, the object must be illuminated by a spectrally continue source. In this case, specific wavelengths are absorbed by an object due to the atomic properties to absorb the frequencies that match the energy difference between two orbitals.

1.3.1 The diffraction gratings

Diffraction gratings exist in a large variety considering shape, spectral range, and other parameters, but there are two primarily categories in reference to the manufacturing process. The first category is the ruled gratings, which are produced by forming grooves on a reflective

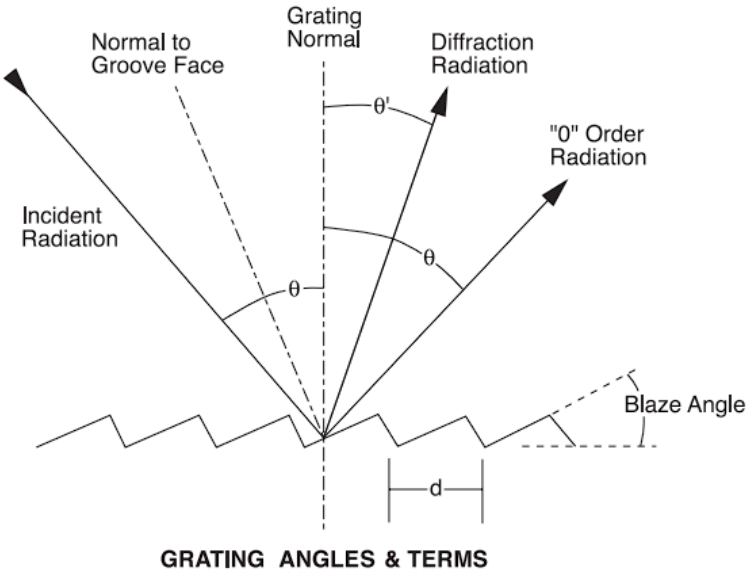

Figure 1.5: Reflection of an incident ray performed by a diffraction grating

surface with a diamond tipped tool. This process typically uses polish substrate on a glass or copper surface, with a coating layer applied through vacuum deposition. The grating is ruled to form parallel and equally spaced grooves. The second category is the holographic grating, which are produced with a photolithographic process to create an interference pattern. The surface is covered by a photosensitive layer and, then, exposed to monochromatic and coherent laser beams that creates a sinusoidal pattern of fringes. At the end, the surface is coated with a reflective material. The main difference between the two processes is the quality of the diffraction grating. Typically, ruled gratings have a high efficiency, but show the presence of ghosts. While holographic ones are less efficient, but have a more uniform groove form and spacing, and also less stray light due to the fact that the production is optical and not physical. The two categories are shown in Figure 1.6.

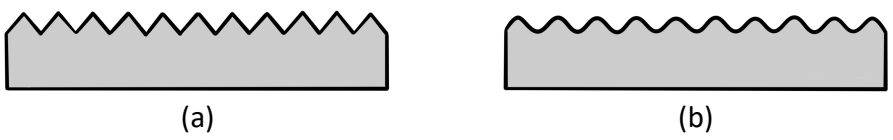

Figure 1.6: (a) Ruled diffraction grating (b) Holographic diffraction grating

In general, the spectral dispersion, generated by a reflective diffraction grating, is described by the Equation 1.11.

$$n\lambda = d(\sin\theta + \sin\theta') \tag{1.11}$$

where:

n is order of diffraction.

λ is the wavelength.

θ is the angle formed between the normal of the surface and the coming ray.

θ' is the angle formed between the normal of the surface and the diffracted ray.

Another variant of the diffraction grating is the transmission grating, in such case, the equation is different as shown in the Equation 1.12.

$$n\lambda = d(\sin\theta - \sin\theta') \tag{1.12}$$

The last important category of diffraction grating is the echelle kind. This category has a lower groove density, commonly used for high incidence angles or cross-dispersed high-resolution spectrographs.
The main parameters considered in the choice of a diffraction grating are:

- Groove spacing: the distance between two grooves. This parameter is fundamental in the grating equation.
- Blaze angle: the angle formed between the grating surface and the local surface on the groove.
- Resolving power: it is defined by the ability to spatially resolve two wavelengths. Two wavelengths are resolved when the peak of a wavelength coincides on the minimum of the second one. The resolution is calculated with the Equation 1.13.

$$R = \frac{\lambda}{\Delta\lambda} = nN \tag{1.13}$$

where:

n is the diffraction order.

N is the number of illuminated grooves.

- Diffraction efficiency: the ratio between the power of the light diffracted in a specific direction and the power of the incident light.
- Spectral range: the wavelength range in which the diffraction grating operates. The high limit is defined by two times the groove period.
- Stray light: the light diffused by a diffraction grating because of the imperfections of the diffraction surface.

2

Introduction to HYPSOS

The HYPerspectral Stereo Observing System (HYPSOS), shown in Figure 2.1, is a prototype for remote sensing able to give simultaneously both 3D spatial and spectral information of the observed target. The instrument is designed to be compact and with reduced mass in order to be compatible with small satellites application, as planetary exploration, or terrestrial environments monitoring.

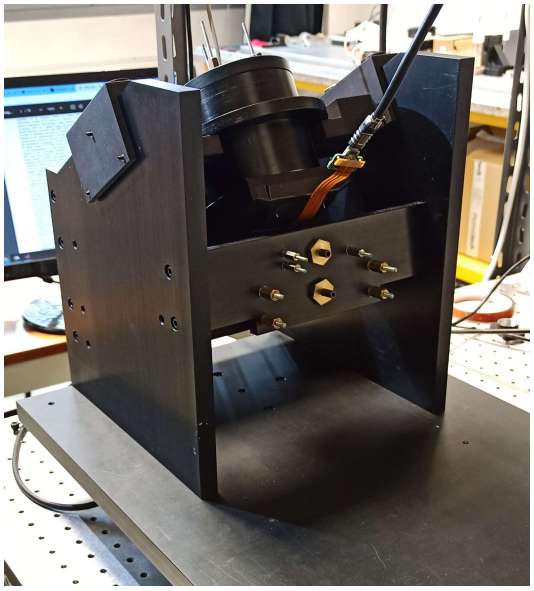

Figure 2.1: HYPSOS during a step of the alignment process

HYPSOS optical design is inspired by BepiColombo's on board stereo camera STC. The prototype consists in two Schimdt-Pechan prisms (SPP), one per channel, and a TMA telescope. The light beam passing through the two channels creates two images on the same focal plane. The light, then, feeds a spectrometer through a double entrance slit, 22 μm wide and 8 mm long for each aperture and separated by 1 mm. The image is spectrally dispersed by a diffraction grating that reflects the light on a bidimensional detector where it is collected. Thanks to the use of a reflecting telescope, HYPSOS can be used over a larger spectrum than STC, from ultraviolet to mid-infrared. In fact, the configuration allows to extend the spectral range adding a second spectrometer. An UV extension would be not suitable with the SPPs, while in the infrared there would be not such concern. A schematic representation of HYPSOS optical design is shown in Figure 2.2.

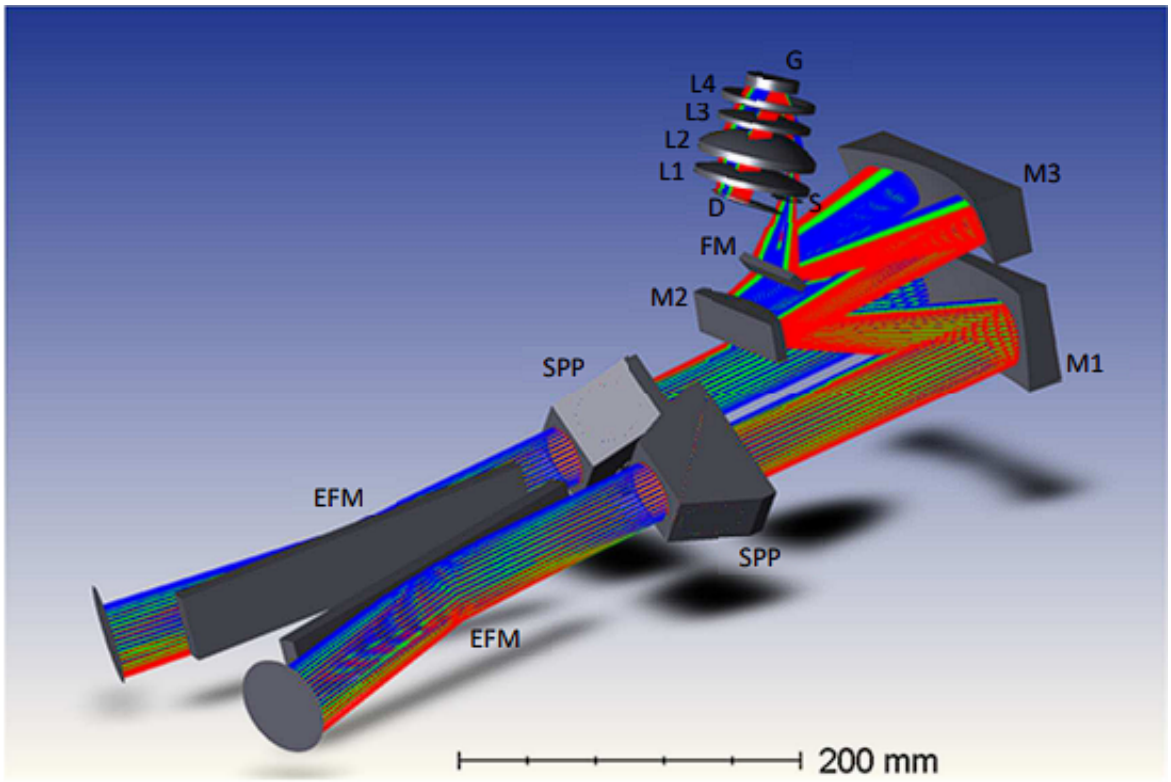

Figure 2.2: HYPSOS simulated on Zemax

Typically, in satellite applications, a standard nadir pointing two-cameras pushbroom stereo system has two channels: one forward and one backward along the flight path of the satellite, as shown in Figure 2.3. In HYPSOS, the new configuration with the two SPPs provides rotation of

90 degrees of the two FoV and allows to use a single entrance slit for the spectrometer. Otherwise, the design would be more complex due to the necessity of two separate entrances. Moreover, the two FoV's enter in the same spectrometer in different positions and crosstalk is avoided due to stigmatic properties of the instrument. The rotation of HYPSOS FoV is shown in Figure 2.4.

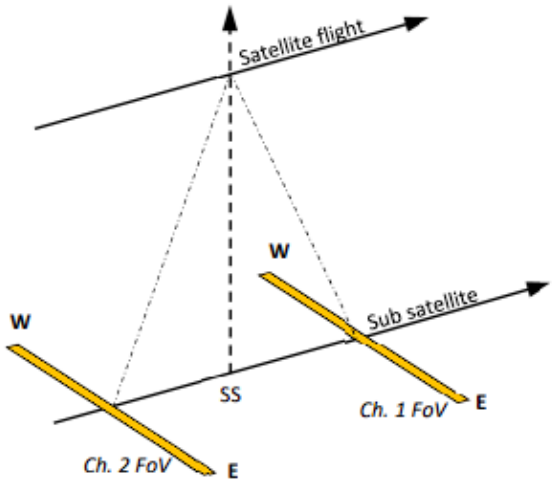

Figure 2.3: HYPSOS FoV in a satellite application

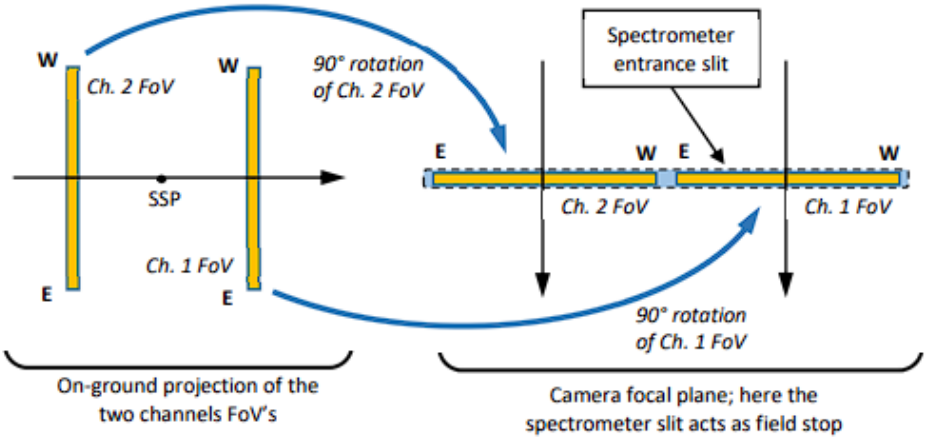

Figure 2.4: Rotation of the two FoV

Almost all the optical elements have been realized by Italian companies, such as Lobre for the lenses and Tecnottica for the mirrors. The diffraction grating is a catalogue one, and has been bought by Richardson Gratings.

2.1 HYPSOS telescope

HYPSOS telescope is a TMA with an additional folding mirror, as shown in Figure 2.5. Two Schimdt-Pechan prisms (SPP) are positioned before the telescope with a 45 degrees tilt to provide rotation of 90 degrees of the FoV. The telescope has a focal length of 245 mm and its optical design consists of three mirrors (M1, M2, M3) and the folding mirror (FM). The distances between mirrors are 135 mm for M1-M2 and M2-M3 and 225 mm for M3-FM. From the folding mirror to the focal plane, the distance is 41.73 mm. The TMA is almost diffraction limited at the longest wavelengths. Concerning HYPSOS aperture stops, one per channel, their diameter is 35 mm, and are located before the SPPs. The nominal FoV of HYPSOS is 18.5 arcsec x 1.87°, where the across track FoV is $(20.125 - 22)°$. The innermost field entering the instrument is tilted by 0.125° respect to the TMA axis, while the outermost is tilted by 2°.

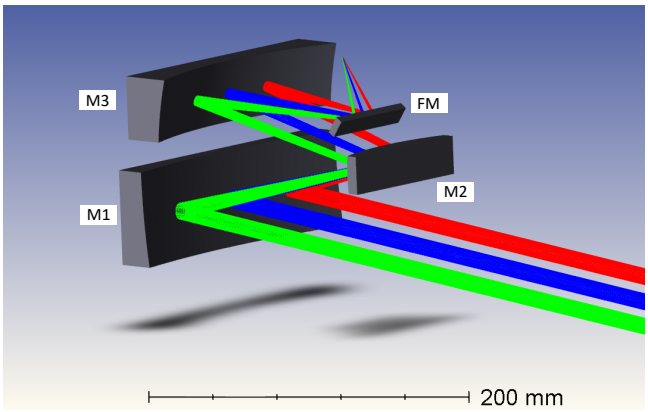

Figure 2.5: HYPSOS TMA on Zemax

The optical elements of HYPSOS telescope are described in the Table 2.1.

M1	Concave hyperbolic surface Radius curvature: 467 mm Conic constant: -1.474
M2	Convex spherical surface Radius curvature: 141 mm
M3	Concave oblate ellipsoidal surface Radius curvature: 117.5 mm Conic constant: 0.198

Table 2.1: Characteristics of the telescope's mirrors

2.2 HYPSOS spectrometer

HYPSOS spectrometer is positioned at the end of the TMA and has a 1x magnification. The light enters from the slit aperture previously described and goes through a system of lenses described in the Table 2.2. This configuration allows to a percentage higher than 80% of the monochromatic energy to be inside a box of 22 μm, the same size of the slit width. In addition, the plate scale factor on the focal plane of the spectrometer is 33.7 nm/mm, meaning that it is possible to resolve spectrally up to 1.5 nm, considering a 22 μm sampling. The spectrometer's optical design is shown in Figure 2.6.

L1	Piano convex lens, material: SK5 R: 84.14 mm, Thickness: 10.5 mm
L2	Piano convex lens, material: BK7 R: 50.78 mm, Thickness: 19 mm
L3	Piano convex lens, material: BK7 R: 91.84 mm, Thickness: 7.4 mm
L4	Meniscus lens, material: BK7 R: 104.4 mm, Thickness: 3.2 mm

Table 2.2: The lenses of the spectrometer and their characteristics

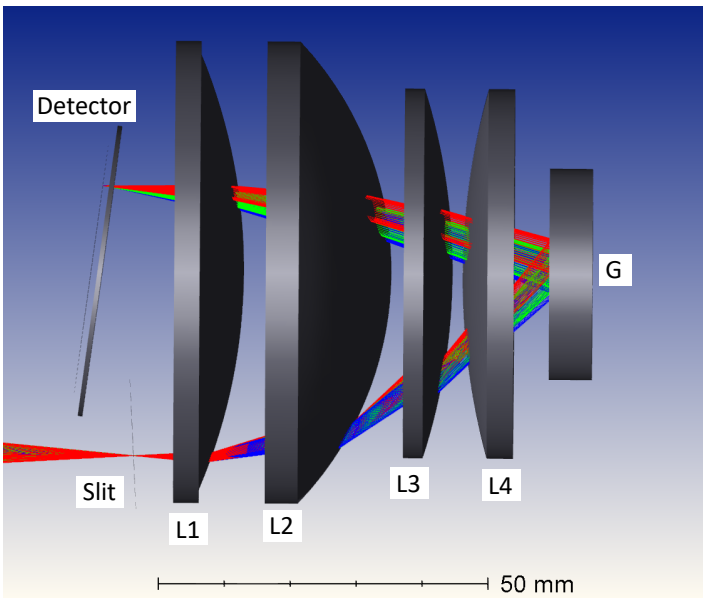

Figure 2.6: HYPSOS spectrometer on Zemax

2.2.1 HYPSOS diffraction grating

HYPSOS diffraction grating is a Richardson Grating concave holographic reflection grating ideal for the spectral region between 200 nm and 800 nm and it is shown in Figure 2.7. Its position is on the opposite side with respect to the entrance aperture of the spectrometer, and diffracts the coming light in its spectral components to the detector. The spectral dispersion is performed through grooves on the reflective area. The characteristics of the diffraction grating are summarized in Table 2.3.

G	Concave spherical grating Radius of curvature: 83.7 mm Ruling density: 678 $1/mm$

Table 2.3: Characteristics of the diffraction grating

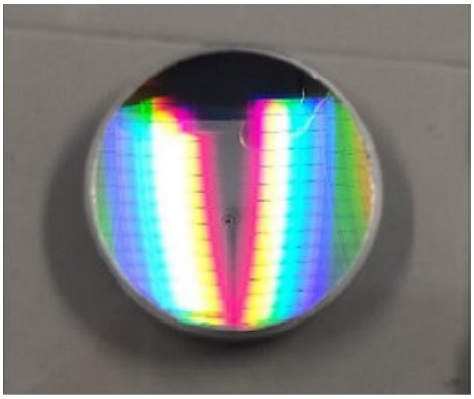

Figure 2.7: HYPSOS diffraction grating

2.2.2 Slit manufacturing

The spectrometer entrance slit has little apertures of the size of 22 μm x 8 mm. The manufacturing process consists of different stages. In the beginning, an electron beam lithography is performed on a Si_3N_4-Si-Si_3N_4 sandwich. Then, through the reactive ion etching method apertures are realized on the Si_3N_4 layer. Finally, with a KOH etching process, the 400 μm thick 100-silicon substrate is removed. In Figure 2.8, the slits are shown during the final manufacturing phase.

With the same technique, many other slits have been realized, including a slit with 8 squares apertures of 22 x 22 μm^2 located as shown in the Figure 2.9 (a). Such slit has been used to analyse the performance of HYPSOS spectrometer during the alignment and characterization process.

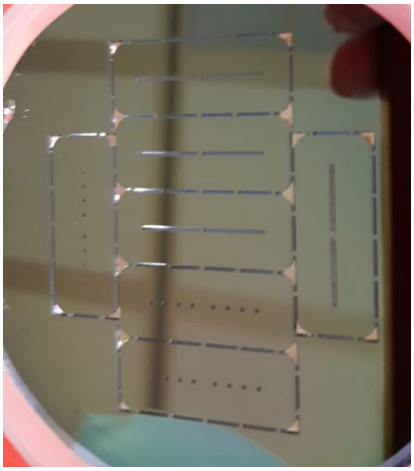

Figure 2.8: HYPSOS slits during the final manufacturing phase

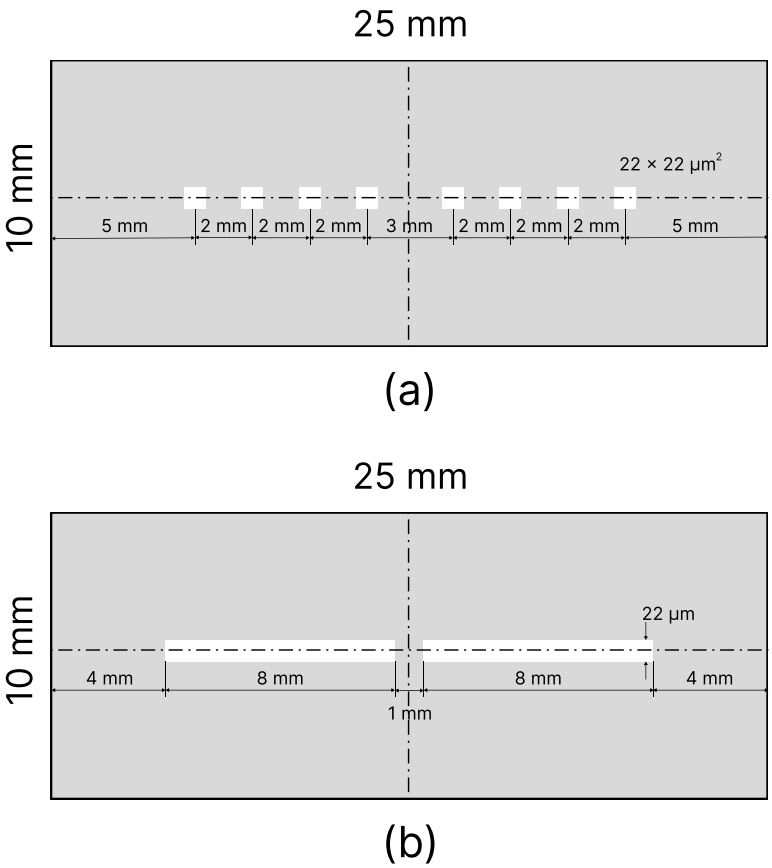

Figure 2.9: Scheme of the slit with the pinhole (a), and the slit required by the design (b)

2.3 HYPSOS detector

The detector is a Sony flat CMOS 6480x4856 with a pixel size of 3.45 x 3.45 μm^2, shown in Figure 2.10. The sensor is located on the same side of the aperture where the light enters the spectrometer, and it is positioned to collect completely the working spectral portion of HYPSOS. The detector has a 12 bit ADC and allows binning and windowing. The push-broom acquisition mode is allowed by the maximum frame rate of 12.1 frames per second. The characteristics of the detector are described in the Table 2.4.

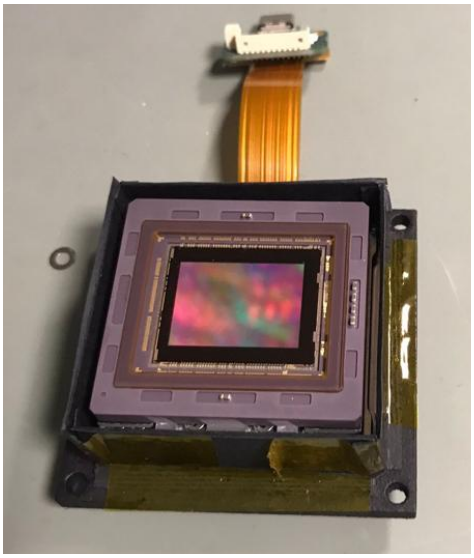

Figure 2.10: Image of HYPSOS detector with one of the mask created during the straylight analysis

Device Structure	CMOS image sensor
Image size [pixel]	6480 (H) x 4856 (V)
Pixel size	3.45 x 3.45 μm^2
SNR$_{max}$ [dB]	39.7
ADC resolution	12 bit

Table 2.4: Main characteristics of the detector

3

Experimental setup

All the components have been characterized on an optical table that provides a solid and stable base. One of the main instruments used during the process of alignment and characterization is a HeNe laser beam arranged parallel to the table, and with wavelength of 633 nm. The diameter of the laser beam is increased by a 20x beam expander which also provides the collimation of the laser beam. Then, the light goes through an iris which allows modification of the diameter of the beam. An image of the setup is shown in Figure 3.1.

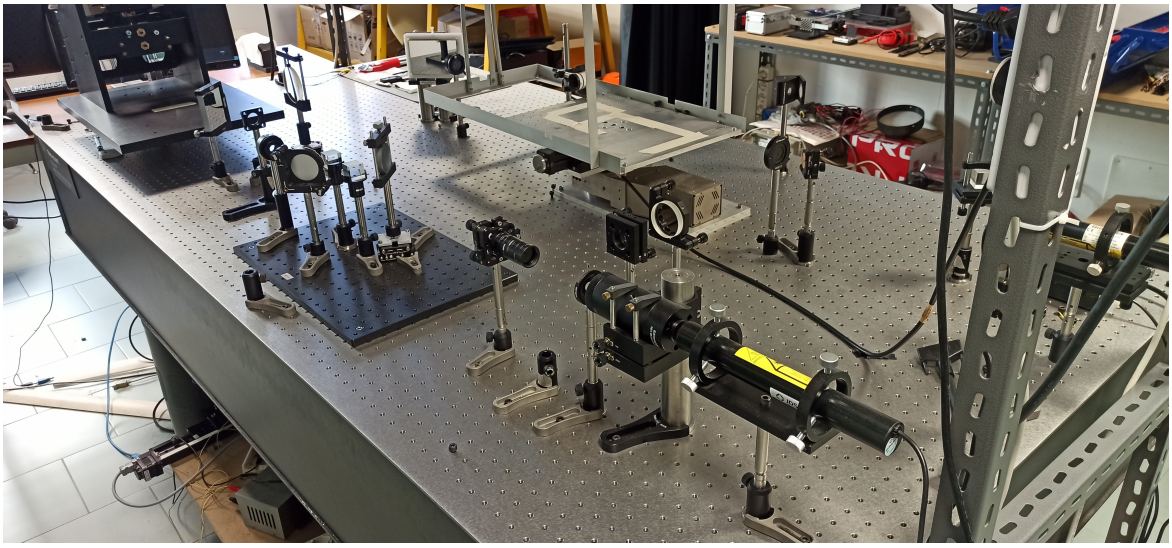

Figure 3.1: Image of the optical setup

To achieve a complete characterization and alignment of the telescope, it has been necessary to prepare a setup with two different paths for different purposes, and they are described in this chapter. Both the setups use the same laser source.

3.1 General procedure for the alignment of a lens

The main procedure to assure the correct alignment of irises and lenses is the autocollimation method, shown in Figure 3.2. It consists in the use of a flat mirror which reflects back the laser beam, and the position of a lens without any deviation of such beam. Initially, the mirror must be placed, so the laser beam returns to the source. It is a condition that can be achieved only when the flat mirror is perpendicular to the beam itself. After placing a lens between the laser and the mirror, eventual variations of the laser beam path, caused by tilt or decentre of the optical axis, may be better observed. The lens must be shifted and tilted with precise movements to achieve absence of variation in the light path.

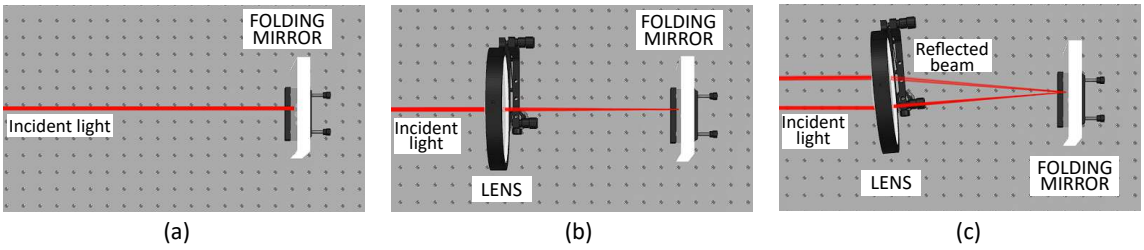

Figure 3.2: (a) Folding mirror in autocollimation (b) Perfectly aligned lens (c) Tilted lens

Another procedure to align lenses is the usage of the back reflection, shown in Figure 3.3. Back reflection is the component of light reflected by reflective surfaces as lenses. The number of spots is equal to the number of reflective surfaces: for example, a singlet lens provides two spots. Such spots provide both information about tilts and decentre of the lens: in fact, tilts and decentre do not permit back reflections to be aligned with the source, and spots to be overlapped. A correct alignment is achieved when back reflections are united in a single spot and aligned with the laser beam.

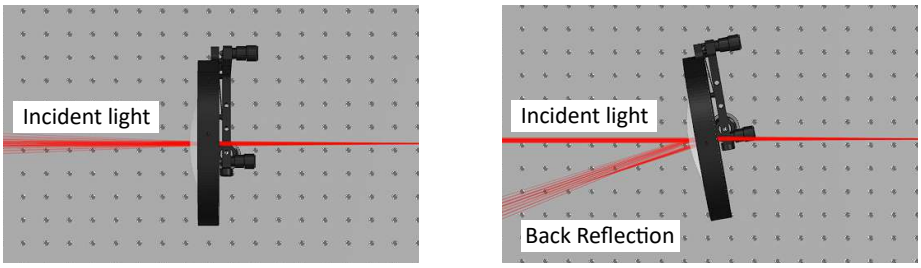

Figure 3.3: Difference in the backreflection between a perfectly aligned lens (a) and a tilted one (b)

3.2 First path

The first path is fundamental to characterize the spectrometer and to align the mirrors of the telescope.

To study the double view of the telescope and the optical system of the spectrometer, the laser beam has been split in three parallel beams using two beam splitters (BS1 and BS2) and two mirrors (LFM1 and LFM2). The purpose of the two lateral laser beams is to correct the position and orientation of the mirrors of the telescope, because they simulate the path of the light through the double view of HYPSOS. While, the central laser beam is mainly used to study the spectrometer. The first beam splitter (BS1) has reflectance of 30% and transmittance of 70%, while the second beam splitter (BS2) has reflectance and transmittance of 50%. This configuration provides equal intensity of light on the three laser beams, which go to the telescope. As convention, mirror LFM1 feeds the channel CH1, while mirror LFM2 feeds the channel CH2. The configuration is shown in Figure 3.4.

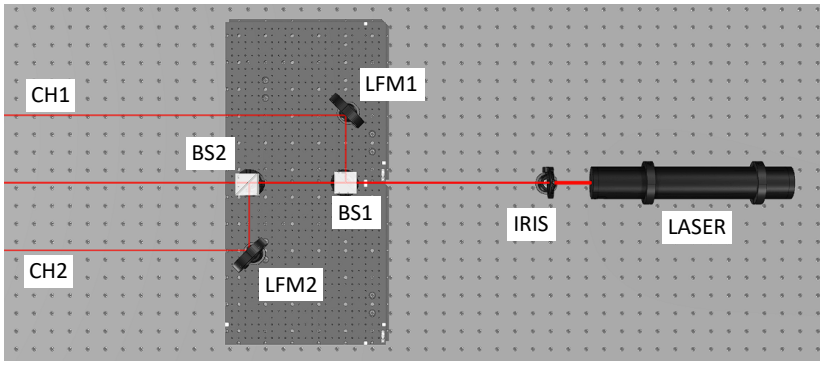

Figure 3.4: Schematic representation of the first path of the setup

The relative distance between the central laser beam and the lateral one, which goes through CH1, is 52 mm along x-axis and 0.5 mm along y-axis. While the other lateral beam has a relative distance of 50 mm along x-axis and -0.5 mm along y-axis. The y-axis is considered with same direction and spatial orientation of the normal of the optical bench. While, x-axis is parallel to the surface of the optical bench and perpendicular to the direction of the laser beam. The different distances of the lateral beams from the central one are caused by a misalignment of the system, but it has been neglected because all the beam are collimated. An image of the first path is shown in Figure 3.5.

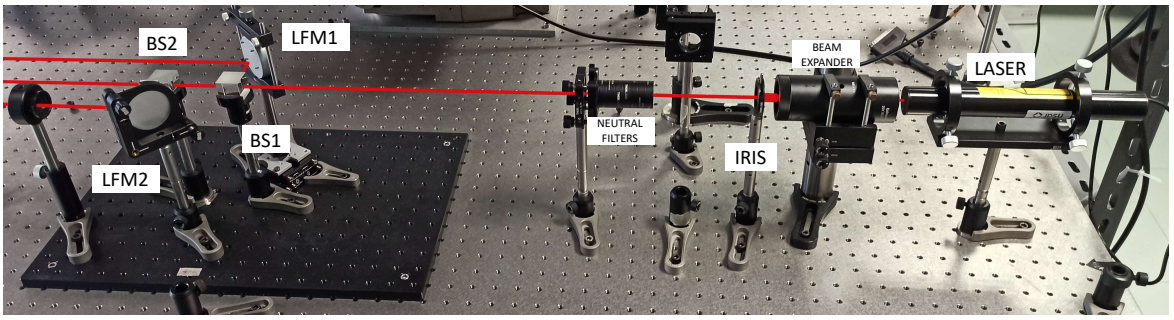

Figure 3.5: First path of the setup

3.3 Test procedure of the first path

The position of the elements which provides the three laser beams has been checked several times during the characterization of the telescope in order to prove the parallelism of the laser beams between each other and with the optical bench. Possible causes of eventual misalignments are the thermal expansion of the supports or vibrations. In order to correct it, a flat mirror is placed between the telescope and the beam splitters to reflect both the central and one of the lateral laser beams. First of all, the central beam is checked to prove being parallel with the optical bench and, then, it is used as reference to place the folding mirror in autocollimation. In this configuration, the parallelism between the two beams can be achieved tilting the lateral mirror (LFM1 or LFM2) until the reflected lateral beam is overlapped with the coming one. In this case, the folding mirror is perpendicular to the lateral beam and the two beams are proved as parallel, because both are perpendicular to the same flat mirror. In Figure 3.6 the initial setup is shown.

The use of a folding mirror allows to study the spots created by the beam splitter on the opposite direction of the lateral mirror, as shown in Figure 3.7. The central reflected beam reaches the

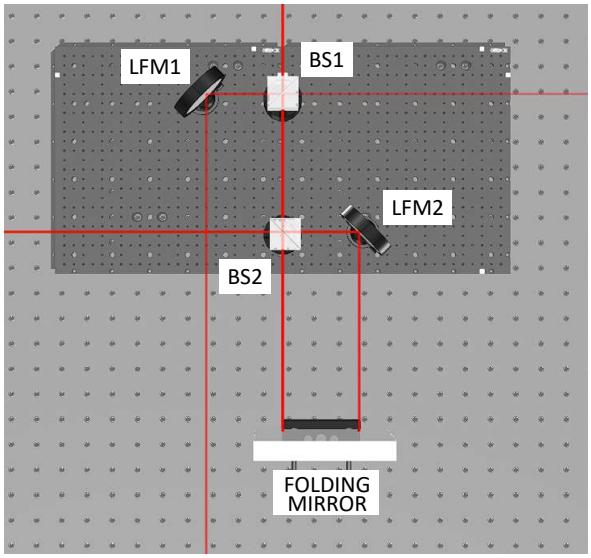

Figure 3.6: Initial procedure to correct the tilt of the mirror LFM2

beam splitter, which partially reflect the beam; the lateral beam, instead, after being reflected by the folding mirror, is partially transmitted by the beam splitter. The two spots can be used as reference for the alignment of the lateral mirror, which is achieved when the spots are overlapped.

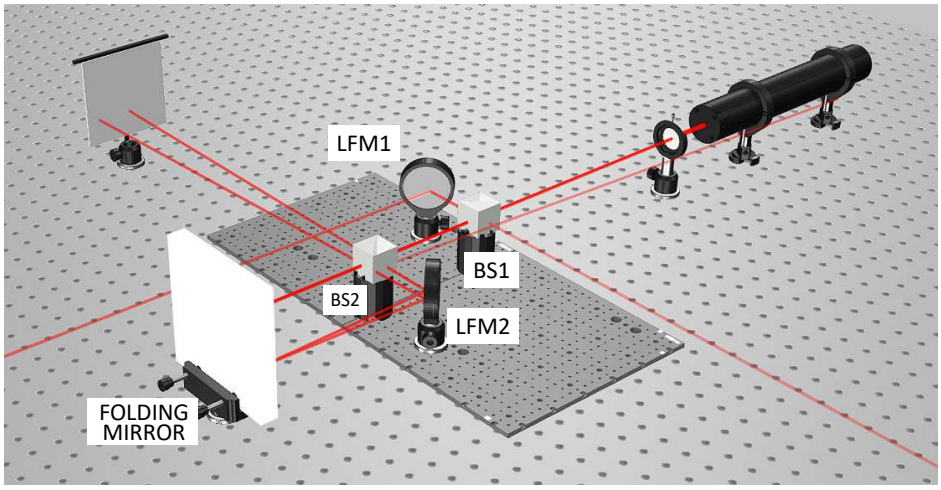

Figure 3.7: Example of the result with a misalignment of the mirror LFM2

The path between the beam splitter and the surface where spots are analysed has been increased in order to improve the precision of the alignment. A camera has been used to provide quantitative data on the alignment. The error in the tilt of the lateral mirrors is below 20 μrad.

3.4 Second path

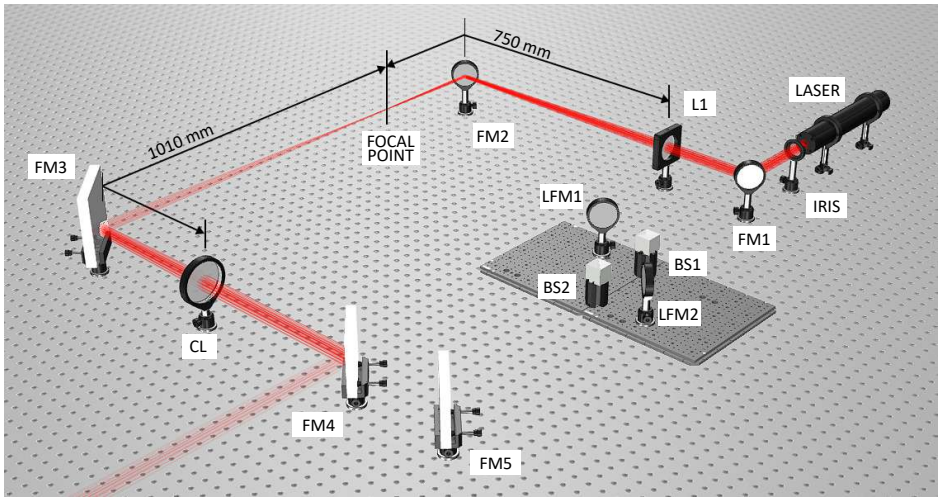

Figure 3.8: A schematic representation of the second path

The second path provides the possibility to increase the diameter of the laser beam to fill completely the entrance pupil of the telescope. In fact, the first path cannot be used for this because the maximal size of the beam is limited by the 1" beam splitter size, while the entrance pupil diameter is 35 mm. A schematic representation of the second path is shown in Figure 3.8. For this purpose, a removable folding mirror (FM1) has been placed in front of the laser to select the second path. Through this path, two lenses are used as a 1.3x beam expander. The first lens is a 2" converging lens with a focal length of 750 mm (L1), while the second lens is a collimator lens with focal length of 1010 mm and a diameter of 3" (CL). The light coming from the collimator lens reaches two folding mirrors. The first one (FM4) can be translated from a position which feeds the channel CH1 of HYPSOS to another one which lets the light feed the other folding mirror (FM5), and consequently the other HYPSOS channel CH2. The motion of the folding mirror is performed by a motorized linear stage controlled by an Arduino Uno board with a A4988 stepper motor driver. The device has been programmed specifically for the setup and can be fully controlled from computer. Two switches located inside the linear stage detect when the translator has reached the limit. The scheme of the electrical circuit and an image of the motion stage are shown in Figure 3.9 and in Figure 3.10. The script to control the Arduino board makes possible to move the mirror with a relative movement, while the absolute position is stored in an external .txt file. In case of necessity, the script can provide the reset of the absolute position using a "home" function. Using this command, the motion stage reaches one switch

and finds the lowest position which does not press the switch. This position can be considered to be fixed, and it has been set as position 0 mm. The script has been written in Python language to be integrated in other future scripts. The complete script is show in Appendix A.1.

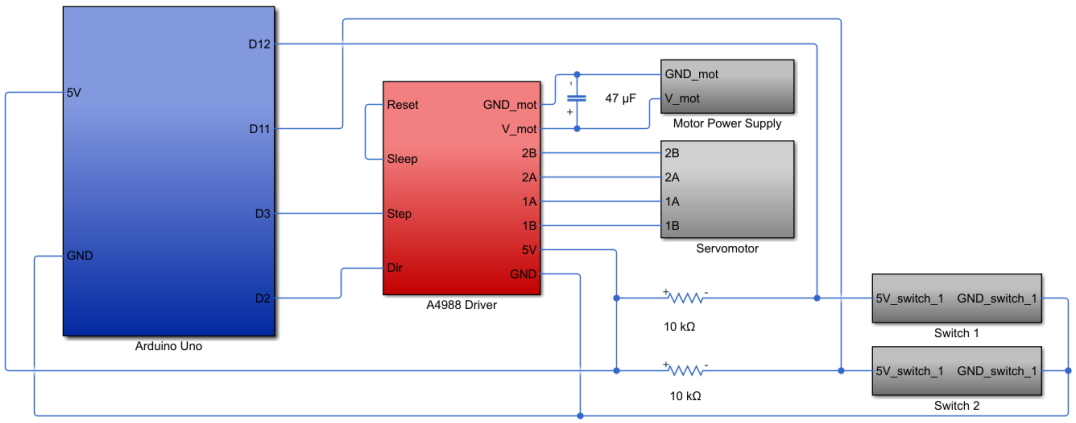

Figure 3.9: Electrical circuit to control the motion stage

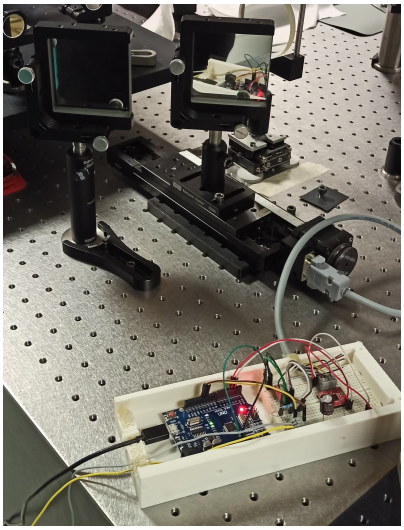

Figure 3.10: An image of the motion stage and Arduino

3.5 Preparation procedure for the second path

The second path has required the alignment of two lenses, the focal point of CL in a specific position, the correct position and tilt of five folding mirrors. Two irises have been placed on the optical bench at the same height to provide an absolute reference for the alignment. With this setup the first two mirrors (FM1 and FM2) have been aligned at 45 degrees respect to the beam, so that the light could pass through the two irises as shown in the Figure 3.11. Then, the third folding mirror (FM3) has been placed with an angle of 45 degrees, after the second iris.

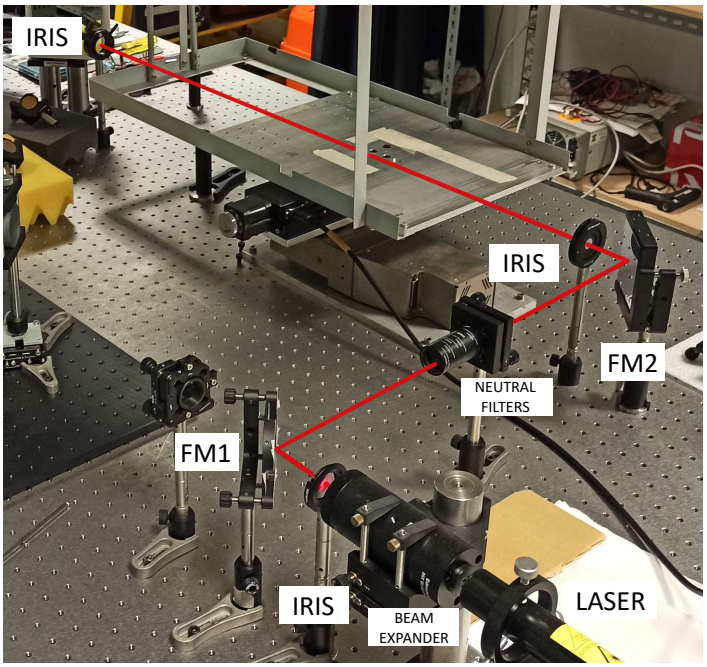

Figure 3.11: FM1 and FM2 alignment using the two irises

Firstly, to align the lenses it has been used the laser coming through the first path. With a mirror the beam has been redirected to FM3 and through the two irises of the second path. Then, the collimator lens CL has been placed. In order to get a correct alignment, the two irises have been checked to assure the absence of deviation of the laser beam after passing through the lens. In particular, the focal point has been set in a specific position, where targets can be placed for further analysis and characterization of the telescope.
Then the second lens L1 has been positioned with the use of the same alignment method of the collimator one. After the lenses have been aligned, the first path has been used to place two

mirrors in autocollimation with the laser beams. Then, the mirrors FM4 and FM5 have been placed and tilted, until the others two mirrors are in autocollimation with the laser beam from the second path. This process is shown in Figure 3.12

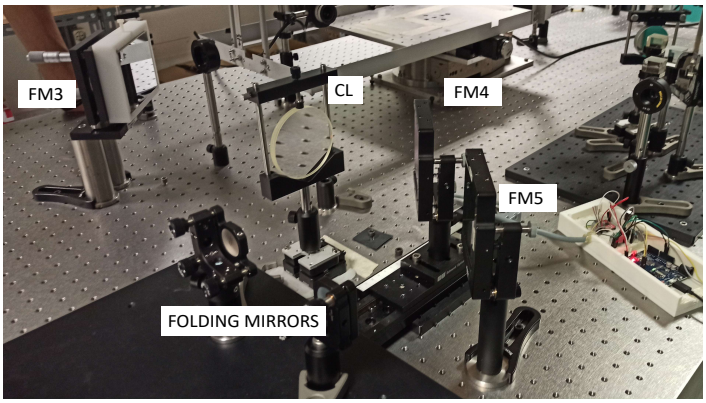

Figure 3.12: FM4 and FM5 alignment using two mirrors in autocollimation

3.6 Procedures to test the second path

As in the case of the first path, it is fundamental to assure the correct alignment of the second path. A shear plate is used to verify the collimation of the laser beam after passing through the 1.3x beam expander. This provides information on an eventual misalignment of the lenses L1 and CL.
In order to test the mirrors FM1 and FM2, the irises described before can be used as reference for the alignment. The mirrors FM4 and FM5 are removed and placed to use one or the other path, so the correct alignment has to be verified every time the second path is required. To achieve a higher precision in this process, HYPSOS telescope can be used with a camera on its focal plane. With this method, the camera takes images of the spots from the first path, then, using the second path, the mirrors must be tilted until the spots in the new image match with the previous ones. The precision of the alignment is calculated considering the minimal shift that can be analysed, which corresponds to a pixel of the camera. Given the focal length of the telescope, $245\ mm$, and the pixel size of the used camera $5.5\ \mu m$, the precision is:

$$\Delta\theta = \arctan\left(\frac{5.5\,\frac{\mu m}{pixel}\cdot 1\,pixel}{245000\,\mu m}\right) = 22.45\,\mu rad \tag{3.1}$$

4

The spectrometer

4.1 Characterization of the system of lenses of HYPSOS spectrometer

The spectrometer of HYPSOS consists of an entrance slit, four lenses located in a metallic cylinder, with fixed distances between each other; a diffraction grating and a bidimensional detector. Various techniques were used to test the lenses position and orientation and are described in this section. The slit, the diffraction grating and the detector have been assembled and properly aligned after the characterization of the lens system, and the complete system has finally been tested and characterized.

4.1.1 Setup

All the procedures to study the spectrometer have been performed using the first path of the setup. In particular, only the central beam is considered. The support of the optical system is made of a vice to hold the weight of the spectrometer, a "V" shape support to adjust the tilt, and a plate to fix the rotation on the y-axis, as shown in the Figure 4.1.

The optical system is aligned to the central beam using the back reflection method. An iris has been placed through the path of the laser beam so that back reflection spots are displayed on it.

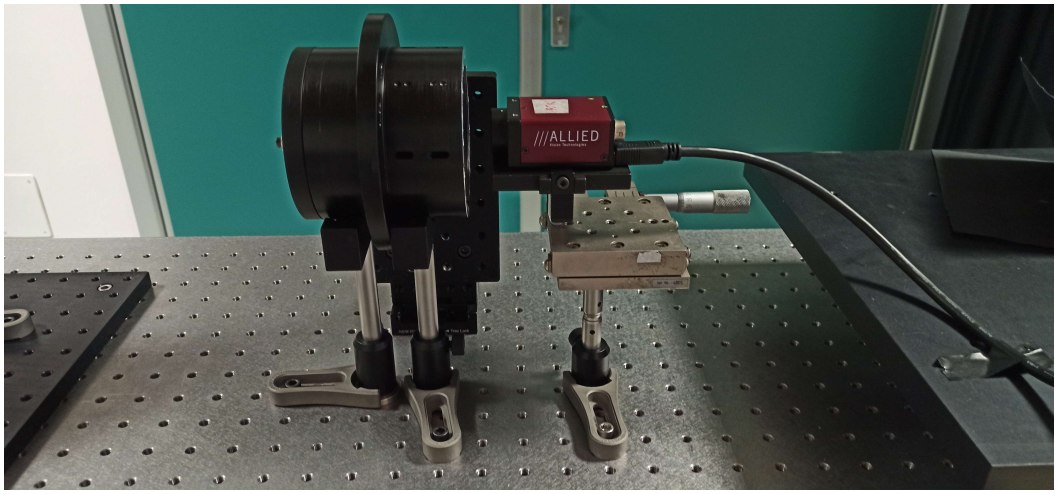

Figure 4.1: Setup used for the analysis of the spectrometer

On the opposite side of the spectrometer, a camera takes images of the spot generated by the laser through the optical system. The information provided by the camera is used to complete the study of the spectrometer's alignment. A schematic representation of the spectrometer's lens system is shown in Figure 4.2.

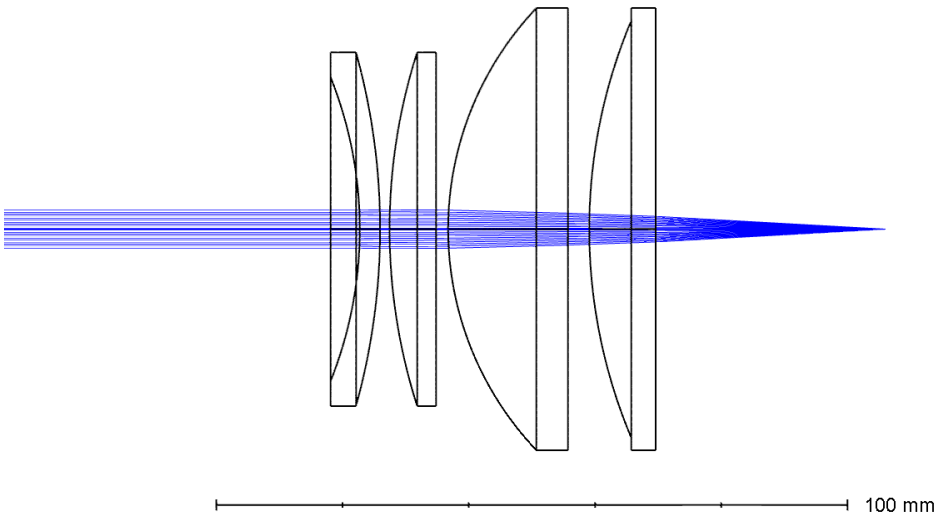

Figure 4.2: Zemax simulation of the spectrometer's lens system

4.1.2 Focal point position

Using the previously described setup, it is possible to find the exact position of the focal point and then, to calculate the focal length of the spectrometer. For this purpose, the camera has been placed over a precise motion stage and then, moved until the spot in the image reaches its smallest size.
Both the distance from the spectrometer and the dimensions of the spot have been compared to the Zemax simulation.

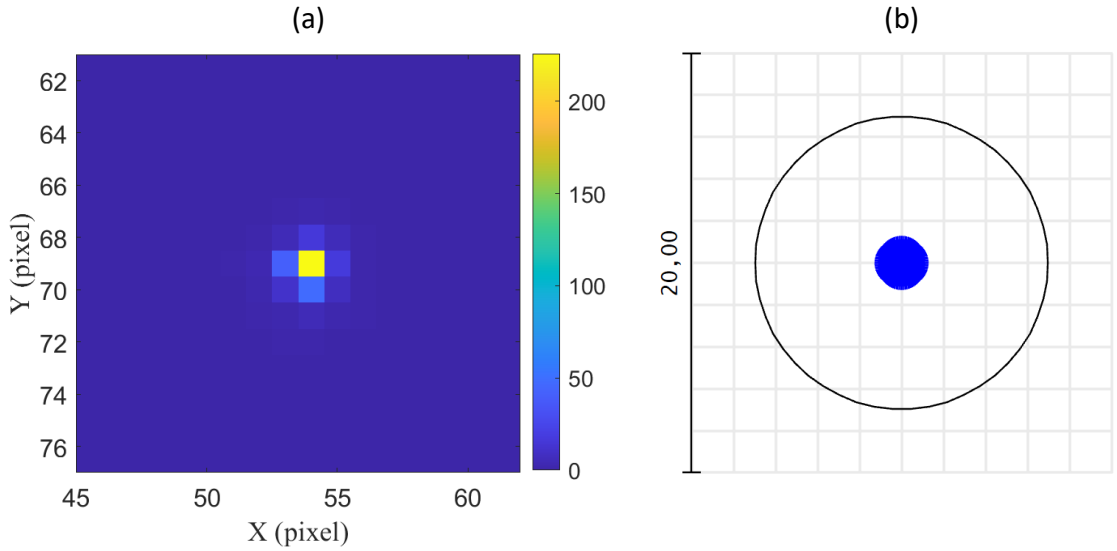

Figure 4.3: Spot in the focal point seen by the camera (a), and simulated on Zemax (b)

The measured focal length is $36.48\ mm$, a result compatible with the focal length calculated by Zemax which is $36.482\ mm$. Concerning the spot dimensions, the diameter of the spot in the focal point is about $2.6\ \mu m$, using a laser beam with diameter of $6.0\ mm$. Such spot size is not accurately measurable due to the pixel-size of the camera which is $9.9\ \mu m$, but the result is consistent with the simulation. The spot size is shown in Figure 4.3.
Using the motion stage, the camera has been moved to three positions further from the spectrometer to compare the size of the spot out focus, shown in Figure 4.4. The shift from a position to another is $0.5\ mm$.

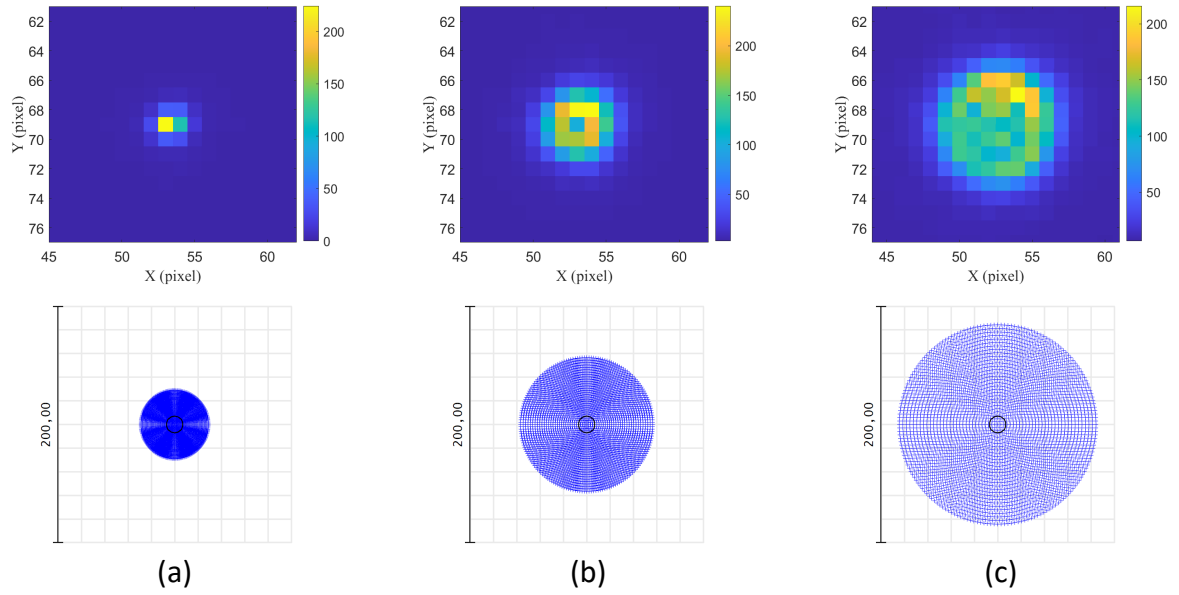

Figure 4.4: Images of the spot size and their simulation with the camera at $0,5\ mm$ (a), $1,0\ mm$ (b) and $1,5\ mm$ (c) from the focal point position

4.1.3 Axisymmetry

The axisymmetry test of the spectrometer has been performed rotating the optical system and taking images of the relative movement of the spot with the same configuration described before. Four images have been taken, shown in Figure 4.5, each one after a rotation of 90 degrees from the previous one. The spot position moved of 9 pixels; and considering the distance of the camera from the spectrometer, the angle of deviation of the laser beam has been estimated as below 0.03 degrees. A probable cause of the shift may be accidental tilts of the spectrometer during the rotation.

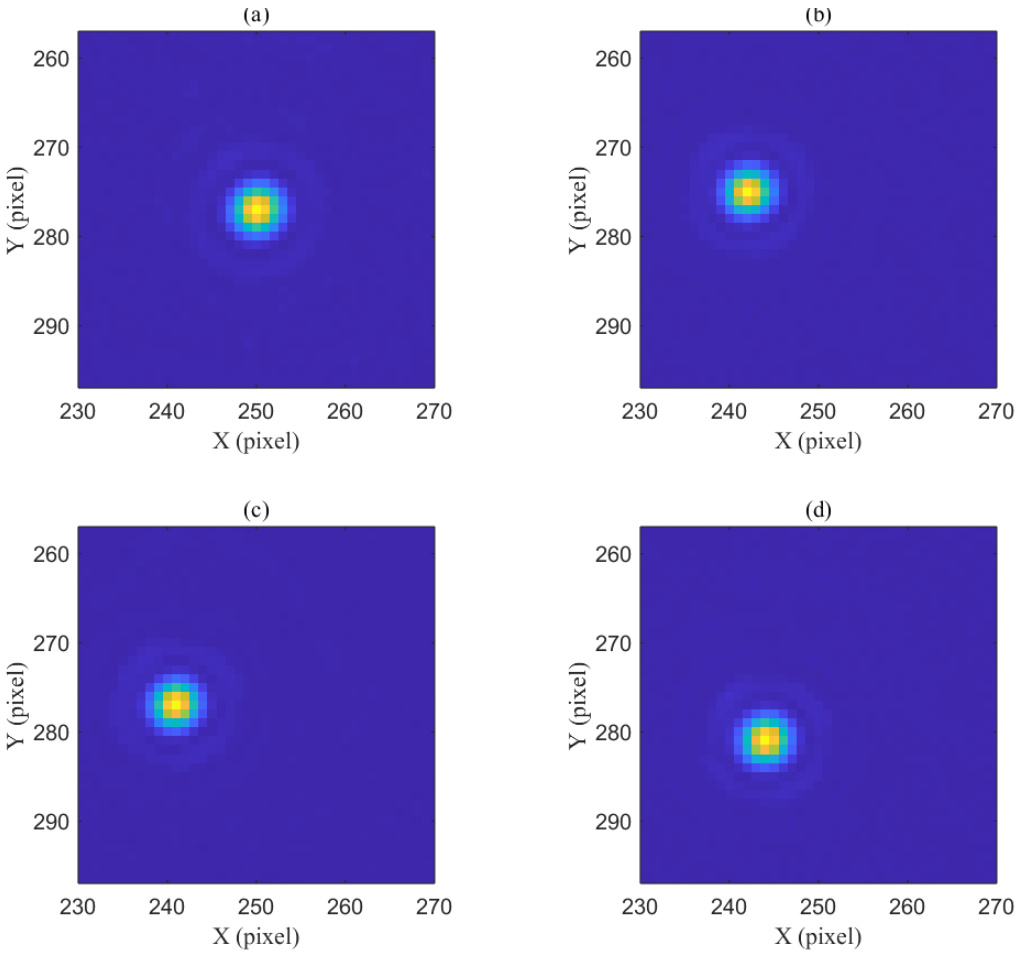

Figure 4.5: Images of the spot after the spectrometer has been rotated of 0 degree (a), 90 degrees (b), 180 degrees (c) and 270 degrees (d) around the optical axis

4.2 Alignment of the diffraction grating

In the optical scheme of the spectrometer, the diffraction grating is aligned with the other lenses in a fixed position. Unlike lenses, the diffraction grating requires a precise inclination above z-axis, or the optical axis, because it determines the direction to which rays are spectrally dispersed. A schematic representation of the spectrometer with the diffraction grating is shown in Figure 4.6.

The diffraction grating is attached to a circular support with three threaded rods and nuts, which connects it to a spectrometer's circular mechanical element. The three threaded rods provide also the possibility to tilt the element around x-axis and y-axis. A ball point screw determines the

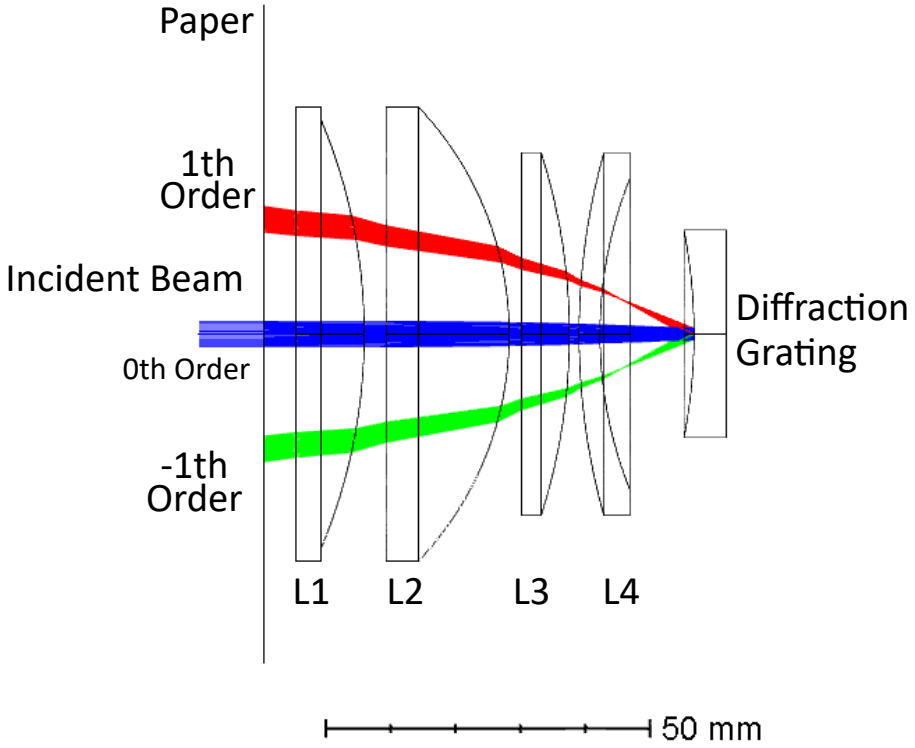

Figure 4.6: Zemax simulation of the configuration used to align the diffraction grating

position of the component along z-axis. The circular support of the spectrometer is removable and is connected to the optical system using tree socket head cap screws, which allow to adjust the tilt around z-axis, rotating the mechanical element.

4.2.1 Procedures for the alignment of the diffraction grating

The setup required for the alignment of the diffraction grating is almost the same used for the characterization of the spectrometer's lenses. The main difference is the presence of a millimeter paper with a hole in the center, attached to the frontal part of the spectrometer. The hole in the center allows the coming beam to go through the paper and to reach the spectrometer. Then, the diffraction grating diffracts the light to the paper, where the spots are displayed.
For the alignment, the diffraction grating has been correctly mounted inside its support. Then, it has been connected to the spectrometer.
The design of the spectrometer requires a precise alignment of the diffraction grating. When the light pass through the slit as in the design, the 0th order beam must be blocked by the baffle vanes located between the lenses. Moreover, the direction of spectral dispersion of the light must be

aligned with the pixel columns of the detector. For this purpose, the diffraction grating's support is initially placed to abut against the spectrometer's circular support with the purpose not to allow tilt around x and y axis. The spot positions are shown in Figure 4.7 and described in Table 4.1.

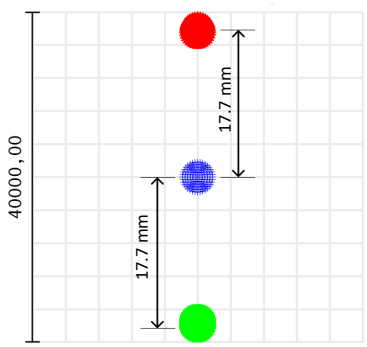

Figure 4.7: Simulation of the spot position with diffraction grating abut against the circular support of the spectrometer

After the correction of the tilt around z-axis, the diffraction grating has been moved 3 mm further from the circular support of the spectrometer to reach the nominal configuration, described in the optical scheme. Using the three threaded rods, the inclination of the diffraction grating's optical axis has been corrected to be aligned to the optical axis of the spectrometer's lenses. The dimension of the spots of first order and their relative position with the coming laser beam has been compared with the simulation in Zemax. Also, the zeroth order reflected ray is studied since it provides information about the tilt of the diffraction grating.The spot positions are shown in Figure 4.8 and described in Table 4.2.

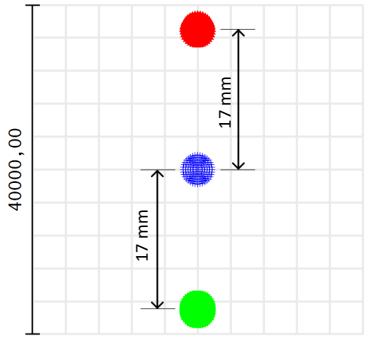

Figure 4.8: Simulation of the spot position with diffraction grating as in the design

The distances between the $\pm$1st and the 0th order are similar with the expected ones from the simulation. The measurement of the diameter of the spots is lower than the simulation one.

Configuration	Distance between 0th and ±1st order [mm]	Spot diameter [mm]
Abutted	17.7	4
As design	17	3.6

Table 4.1: Results from the simulation (laser diameter = 4 mm)

Configuration	Distance between 0th and ±1st order [mm]	Spot diameter [mm]
Abutted	17.5	2
As design	17	1.5

Table 4.2: Results from the assembly (laser diameter = 4 mm)

This can be explained by the fact that the actual beam size is smaller than the one used for the simulations.

4.3 HYPSOS detector

HYPSOS detector has been previously characterized and, for this reason, only the straylight analysis has been performed. An image of the straylight analysis is shown in Figure 4.9.
After the detector has been correctly assembled with the spectrometer, a qualitative analysis of the presence of straylight has been performed. The spectrometer has been illuminated with a halogen lamp and images with different exposure time have been taken. Ideally, the only way light can reach the detector is through the slit aperture. In the same conditions but with such apertures blocked, no ray can reach the surface of the camera. So, the analysis has been performed just covering the slit aperture. The initial images taken by the camera showed the presence of diffuse light on the camera's surface. Covering different zones of the spectrometer, it was possible to identify the apertures where the rays went through the optical elements. One of the main ways in which light reached the detector was the empty space between the sensor's mainboard and the mechanical support which it is attached to. For this reason, a mask of cardboard, Figure 4.10, has been made and placed to block the coming light. Other apertures have been examined and blocked with black duct tape.

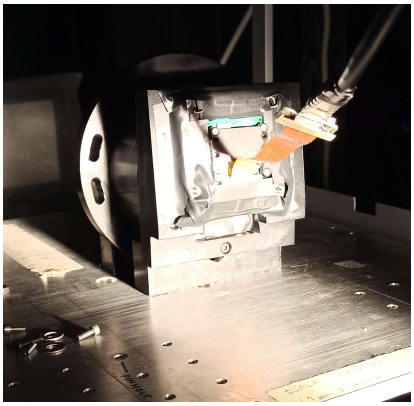

Figure 4.9: Setup used during the straylight analysis

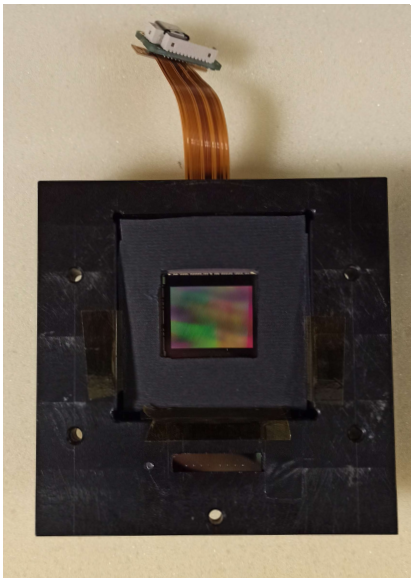

Figure 4.10: The detector after the mask has been placed

Figure 4.11 (a) shows the initial situation on the detector with an exposure time of 8 seconds. The light could reach the top area of the detector illuminating the sector where lower wavelengths are collected. With this configuration, the average DN value calculated on all the pixels was 0.6113, while in the straylight area the maximum DN value was 34. Figure 4.11 (b) shows the final situation after properly covering the path which light goes through: we can see that straylight is no longer detected or does not decrease the quality of the final images.

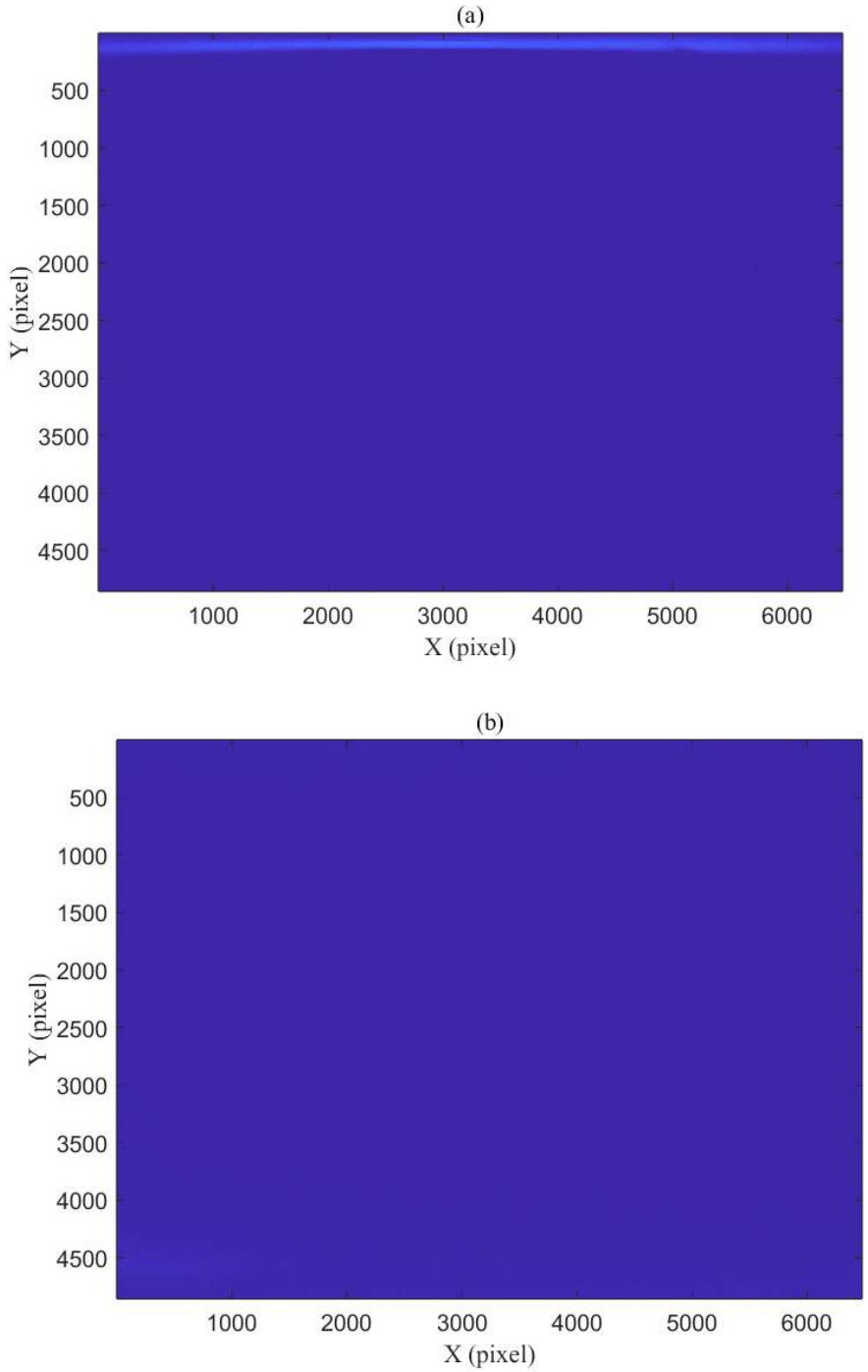

Figure 4.11: Images acquired before (a) and after (b) placing the mask

4.4 Pinhole

Even though HYPSOS spectrometer has a slit with an aperture of 8 mm x 22 μm, a slit with square pinholes of 22 x 22 μm^2 has been used to check the optical performance of the spectrometer. In fact, in this way a point-like source is set on the entrance focal plane of the spectrometer, and the estimation of its aberrations of the dispersion focal plane when illuminated with a spectral lamp gives us a good indication about the spectrometer alignment quality and resolution performance. The incoming light is diffracted by the grating in its spectral components along the detector y-axis, while the detector x-axis, which corresponds to the imaging direction, provides the spatial information.

4.4.1 Pinhole's characterization

A first characterization of the completely assembled spectrometer has been performed to test the correct position of the diffracting grating. In this analysis, spectral lamps are placed in front of the spectrometer. The coming light from the source enters in the optical system through the pinholes. The rays reach the diffracting grating and then, the detector. From this initial configuration it has been possible to study the FWHM in the x-direction. Since the magnification is 1x in the spectrometer system, the FWHM of the spot along the spatial dimension should be equal to the dimension of the aperture. In the initial images, it was possible to notice this value was around 100 μm, while the dimension of pinholes was expected to be 22 μm, as shown in Figure 4.12.

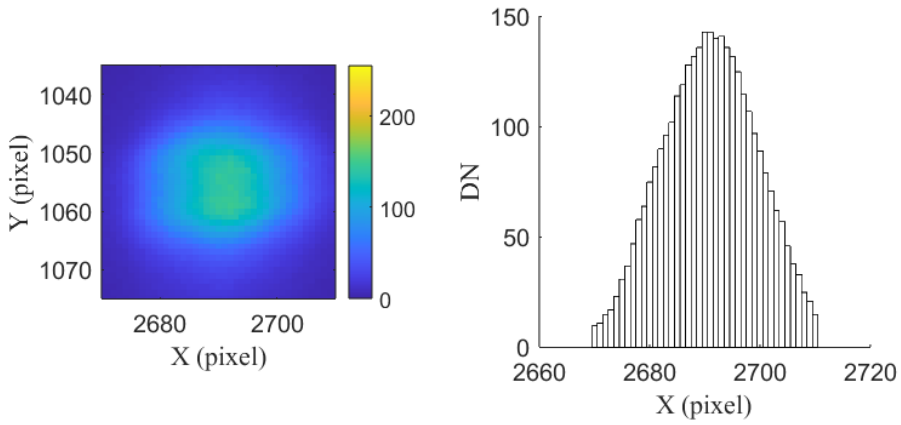

Figure 4.12: FWHM of the spots with the initially used pinholes

The gap between the data has brought to analyse the pinholes dimension using a calibrated microscope. Using a Zeiss AX10 Lab.A1 microscope with a Zeiss AxioCam ERc5s camera, it has been possible to get images and measurements of the pinholes, as shown in Figure 4.13. This provided full characterization of the pinholes. The entrance has size of 22 μm along the spectral dimension and 110 μm along the spatial dimension, while the exit part has size of 550 μm x 550 μm, as shown in Figure 4.14.

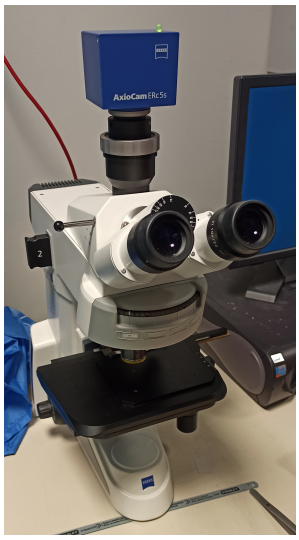

Figure 4.13: The microscope and the camera used to measure the pinhole's size

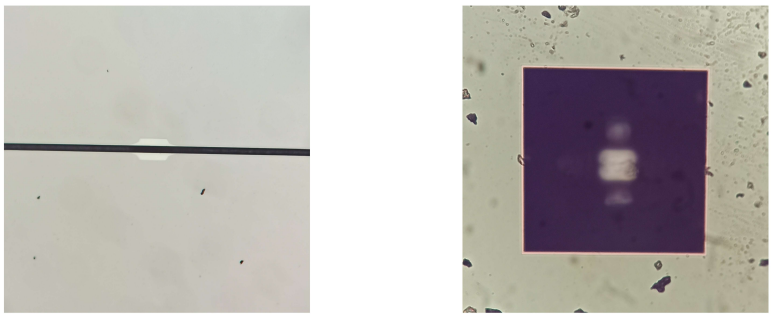

(a) (b)

Figure 4.14: Images acquired from microscope of the initially used pinholes: telescope side (a), spectrometer side (b)

Other pinholes have been characterized the same way to provide information on their size. The entrance has dimension of 22 μm along both spatial and spectral dimensions, while the exit part

has size of $550\ \mu m$, as shown in Figure 4.15.

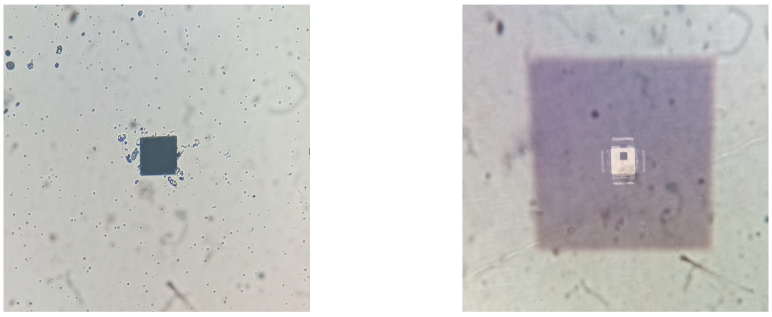

(a) (b)

Figure 4.15: Images acquired from microscope of the $22\ \mu m$ pinholes: telescope side (a), spectrometer side (b)

Using the $22\ \mu m$ pinholes, the spectrometer provides the expected size of the spectral lines along the spatial direction, as shown in Figure 4.16.

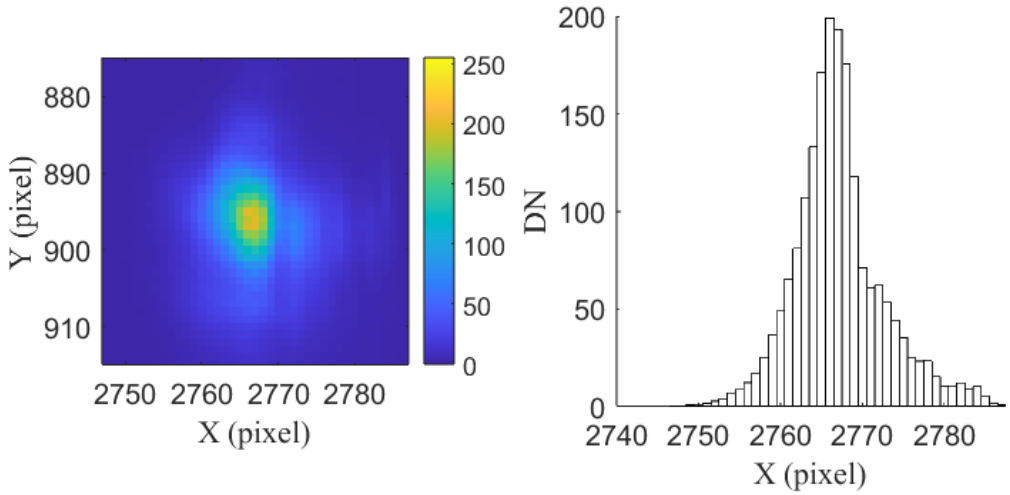

Figure 4.16: FWHM of the spots with the $22\ \mu m$ pinholes [FWHM $\simeq 7$ pixel; pixel size $= 3.45\ \mu m$]

4.5 Spectral performances analysis

Before assembling the spectrometer on the telescope, the performance of the spectrometer has been determined using spectral lamps and studying their spectrum. In order to conduct this analysis, the slit with the pinholes has been assembled. The images acquired have been studied through different MATLAB scripts.
During this measurements, spectral lamps have been placed in front of the spectrometer entrance slit. The taken images have different exposure times in order to make visible dimmer components but avoiding pixel saturation.

4.5.1 Two dimensional gaussian fit

In this configuration, the images show a pattern of spots aligned along the x-direction, or spatial dimension, and y-direction, or spectral dimension. The number of spots along the first direction is eight, as the number of pinholes in the slit. On the other axis, the number of the spots corresponds to the spectral components of the analyzed lamp.
To create the spectral curve, it is necessary to know the exact position of the centroid of each spot in the image, and then, to study their y-coordinates. The method used to find this information is a 2D gaussian fit.
Every image has been studied as a mxn dimensional matrix M, where m and n are the pixel dimension of the image, in this case 6480x4856 corresponding to the detector's pixels. Every element (i, j) of the matrix M has a x-coordinate corresponding to the column i and a y-coordinate corresponding to the row j. The number stored in the position (i, j) is the z-coordinate and it corresponds to the DN value of the pixel (i, j) in the camera.
Analyzing a small portion of the image where there is a spot, it is possible to use the matrix and make a two dimensional gaussian fit using the coordinates x, y and z. The curve allows to find the position of the peak, or the centroid of the spot, with a higher precision.
The initial distribution function used to fit the spot is described in the Equation 4.1.

$$f(x, y) = A \exp\left(-\left(\frac{(x - x_0)^2}{2\sigma_x^2} + \frac{(y - y_0)^2}{2\sigma_y^2}\right)\right) + d \tag{4.1}$$

where:

A is the amplitude.

(x_0, y_0) is the coordinates of the centroid.

σ_x, σ_y describe the spread of the spot along x-axis and y-axis.

d is the offset from the z-axis.

Another distribution function used to analyze the spots is the two dimensional elliptical gaussian function, shown in the Equation 4.2.

$$f(x,y) = A\ \exp\left(-\left(a(x-x_0)^2 + 2ba(x-x_0)(y-y_0) + c(y-y_0)^2\right)\right) + d \tag{4.2}$$

The parameters of the Equation 4.2 allows to calculate the tilt of the major axis of the ellipse, σ_x and σ_y as follow.

$$\begin{aligned} \theta &= \frac{1}{2}\arctan\left(\frac{2b}{a-c}\right) \\ \sigma_x^2 &= \frac{1}{2(a\cdot\cos^2\theta + 2b\cdot\cos\theta\sin\theta + c\cdot\sin^2\theta)} \\ \sigma_y^2 &= \frac{1}{2(a\cdot\sin^2\theta - 2b\cdot\cos\theta\sin\theta + c\cdot\cos^2\theta)} \end{aligned} \tag{4.3}$$

The main difference is the possibility to correctly fit an elliptical spot, while the previous distribution function suits better for circular spots. Despite the increase of precision in the fit, centroid position of the spots are always the same using both the methods.
In the MATLAB scripts, the images are opened and studied as matrixes. Using the function `imbinarize`, it is possible to convert all the matrix elements with a value over or equal a threshold to 1, and values under the threshold become 0. This line leads to the creation of a binary image, where the spots are white, while the background is black. Another function studies the white shapes and calculates their geometrical centroids. Then, a box of 20 pixel is created with the geometrical centroid as center of the square. The fit is performed inside this box to study a single spot in order to avoid decrease of the precision in the fitting, for the presence of other spots in the same fit area.
Fitting this kind of distribution function requires correct initial values that have been calculated as shown in the Table 4.3.

4.5.2 FWHM analysis

Studying the spectrometer, it is possible to understand the correct focal position analyzing the FWHM of the spots along the spatial dimension. Due to the aperture of the pinholes is 22 μm and the magnification of the lenses of the spectrometer is 1x, the FWHM along x-direction is 22

Parameter	Initial value
(x_0, y_0)	(x, y) coordinate of the geometrical centroid
A	Max DN value in the considered area
d	Average DN value in all the image

Table 4.3: Initial value for the fit

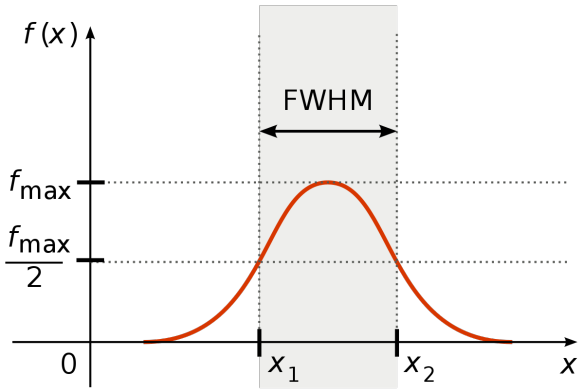

Figure 4.17: FWHM of a gaussian distribution

μm in an ideal configuration. A higher value of the FWHM means that the spectrometer's focal point is not located on the detector or that other misalignment aberrations are dominant.. Some of the reasons of this issue can be a wrong alignment of the diffraction grating or a wrong position of the camera.
Using a similar script to find the centroid of the spots, it is possible to extract the row corresponding to the y-coordinate of the centroids, and to fit the detected spatial profile with a gaussian function in order to calculate the FWHM along the spatial direction. The fitting function is

$$f(x) = a \exp\left(-\frac{(x-b)^2}{2c^2}\right) + d \tag{4.4}$$

whose FWHM is

$$FWHM = 2\sqrt{2\ln 2}\, c \tag{4.5}$$

The obtained FWHM values are different in different portions of the sensor. Different value are obtained analysing other spots. This issue can be solved correcting the tilt and the position of the detector. On average, the measured FWHM are in line with the expected value of 22 μm.

4.5.3 Spectral curve

Every spot corresponds to a spectral component of a spectral lamp and, with the NIST database, it has been possible to know the associated precise wavelength. From this information, the spectral curve can be fitted using the y-coordinate of the centroids of every spot and their corresponding wavelengths. This linear function leads to the spectral curve fit. The fit is performed through a linear fit using the spectral lamps reported in the Table 4.4. The result is shown in Figure 4.18.

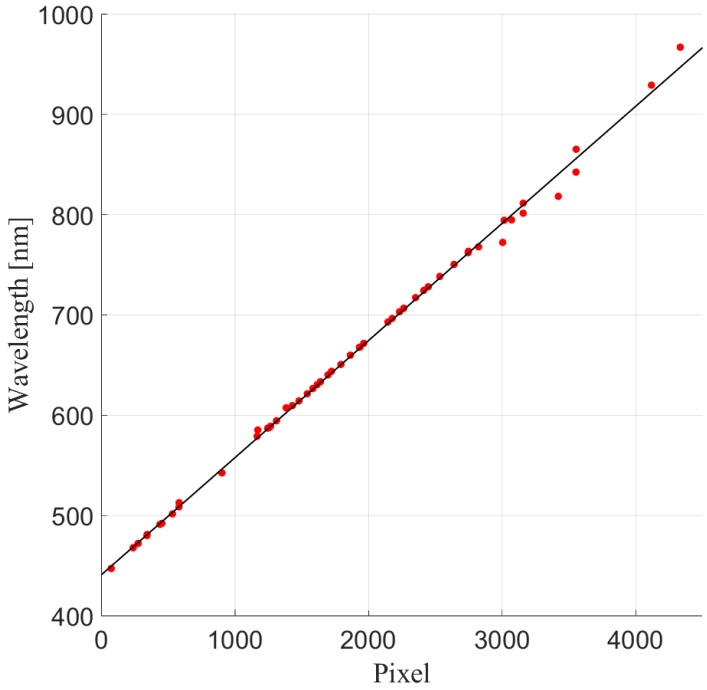

Figure 4.18: Spectral curve

$$y = 0.1168x + 441 \tag{4.6}$$

From the linear fit of the spectral curve, the fit slope is $\Delta\lambda/\Delta x = 33.85\ nm/mm$ and it is calculated as described in the Equation 4.7 considering the camera pixel size. Comparing the result with the expected value of $34.7\ nm/mm$, the percentage error is lower than 2% which is acceptable for HYPSOS applications.

$$\frac{\Delta\lambda}{\Delta x} = \frac{0.1168}{3.45 \cdot 10^{-3}} = 33.85\frac{nm}{mm} \tag{4.7}$$

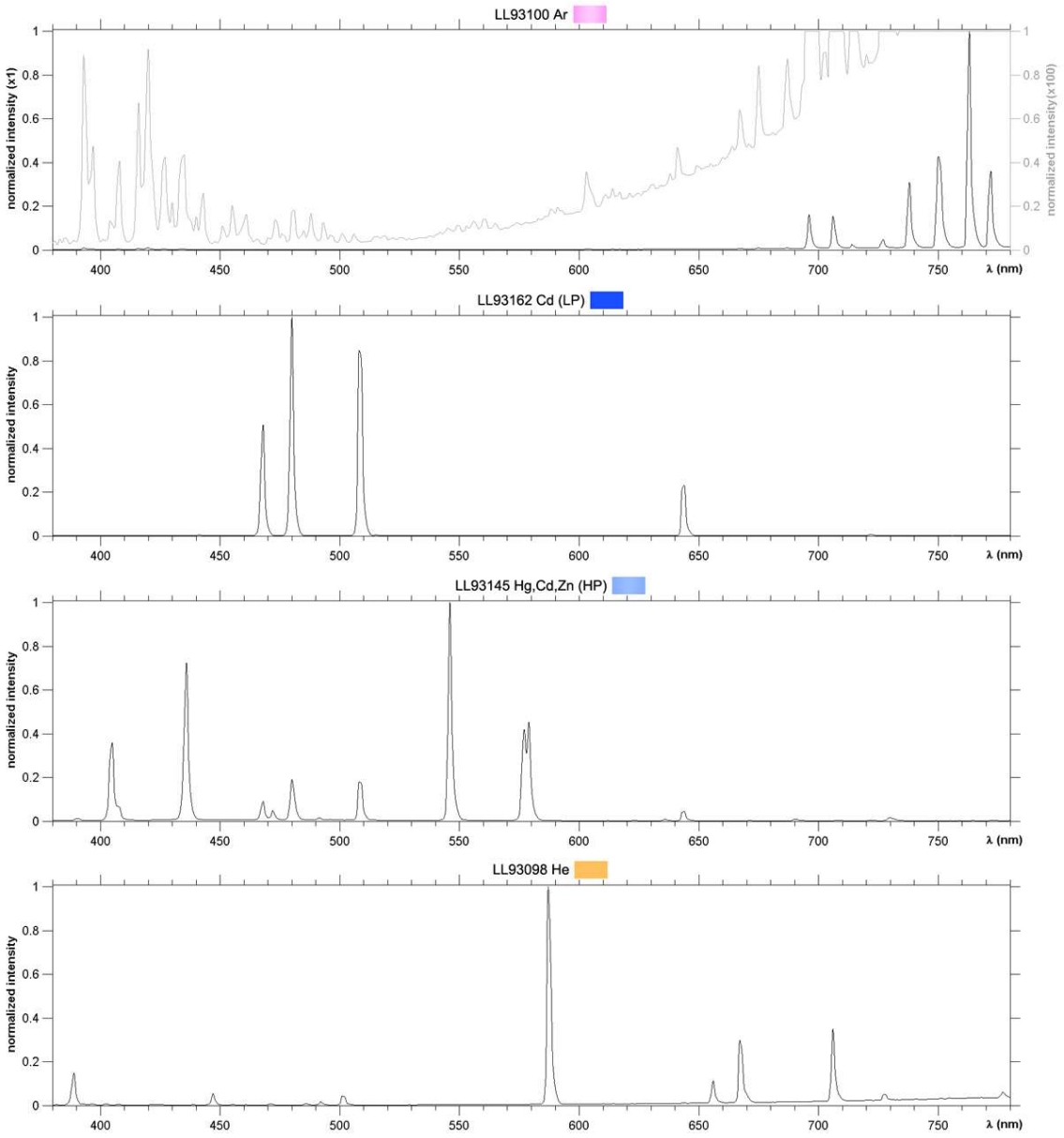
LL93100 Ar
normalized intensity (x1)
normalized intensity (x100)
λ (nm)
LL93162 Cd (LP)
normalized intensity
λ (nm)
LL93145 Hg,Cd,Zn (HP)
normalized intensity
λ (nm)
LL93098 He
normalized intensity
λ (nm)

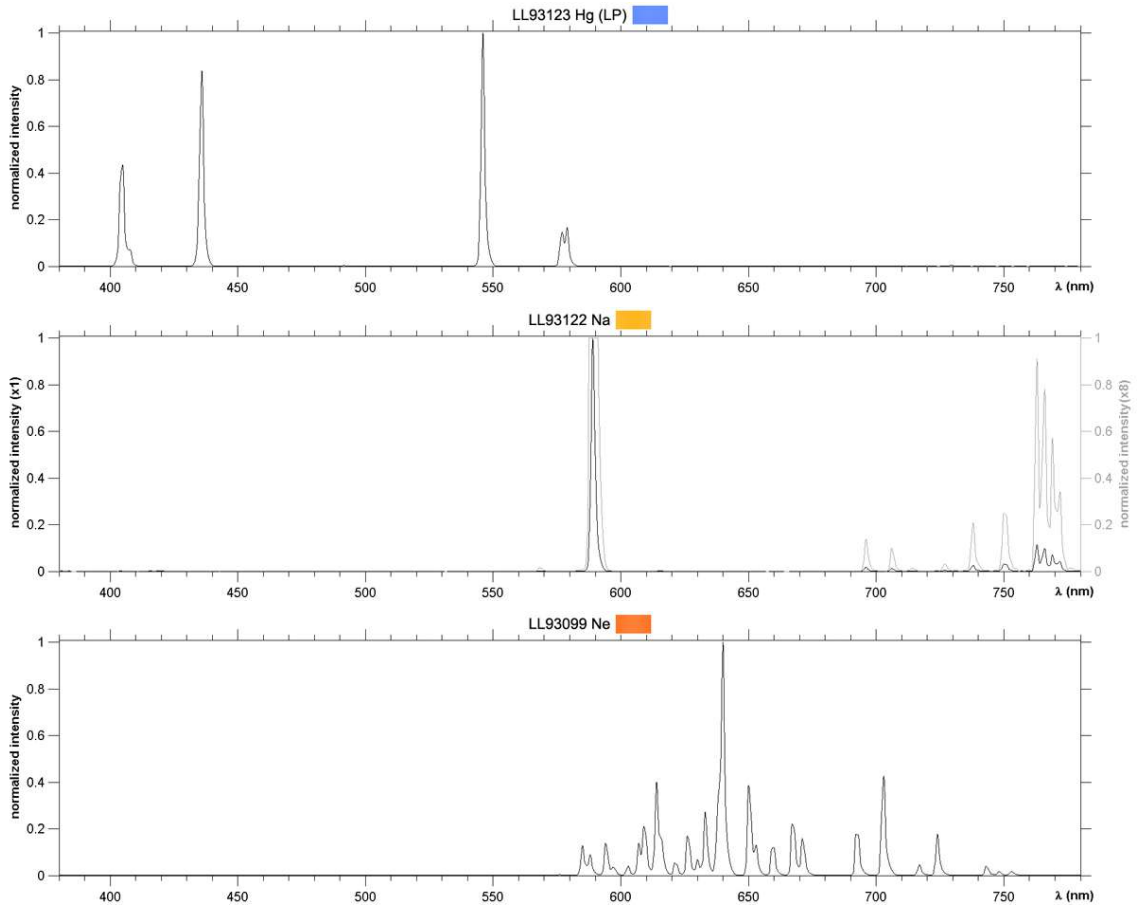

Table 4.4: List of the spectral lamps used for the spectral curve

4.6 Conclusions

The results from the analysis and characterization of HYPSOS spectrometer are in line with expectations. In particular, the optical performance of the lens system are highly similar to the simulated ones. Concerning the FWHM results, they can be improved adjusting the position and tilt of the detector to assure the expected FWHM on all the sensitive area. Another issue observed during the characterization is the fact that the slit can not be placed in a precise position. It is clear that every time the slit is placed, the diffraction grating, and so the detector, are illuminated in different ways. Concerning the straylight, the issue has been solved with a correct mask on the detector. Consequently, the performance of HYPSOS spectrometer globally match with the estimated one or within the tolerance.

5 The telescope

5.1 Mirrors characterization

HYPSOS telescope is a TMA telescope with an additional folding mirror. During the activities in the laboratory it was required the characterization of M1 and M3 to guarantee that their features match the design characteristics. The procedure has been performed comparing the spots created by the light reflected by the mirror with the simulation on Zemax.

5.1.1 Characterization of mirror M1

The setup created for the characterization of M1 is composed of the three laser beams from the first path of the experimental setup, mirror M1 which is assembled inside HYPSOS telescope, and a camera over a linear translation stage. A schematic representation of the experimental setup is shown in Figure 5.1.

The configuration has been studied to reflect the laser beams to the sensor of the camera and to allow an estimation of the relative distance between the camera and the mirror. The camera is moved in precise positions to compare the acquired spots at different distances. Considering the distance of the sensitive area of the camera from the mirror, the shape and size of the spots provide all the information to compare the conic constant of M1 with the one on Zemax simulation.
The images of the spots on the camera and the corresponding simulation on Zemax are shown in Figure 5.2 and Figure 5.3.

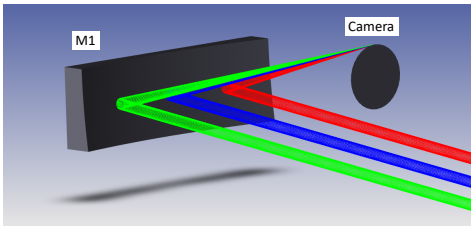

Figure 5.1: Scheme of the experimental setup used to characterize M1

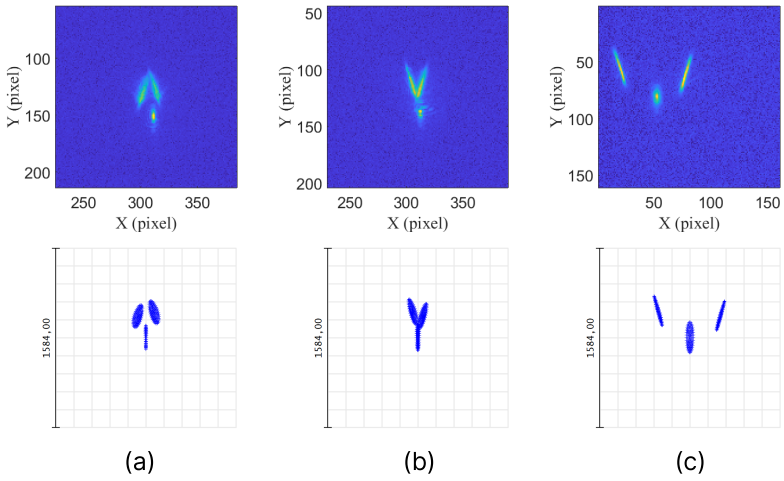

Figure 5.2: Images of the spots and their corresponding simulation with the camera at about $250.8\ mm$ from the M1 plate support (a) and moving the camera $0.5\ mm$ (b) and $1.5\ mm$ (c) farther from the mirror

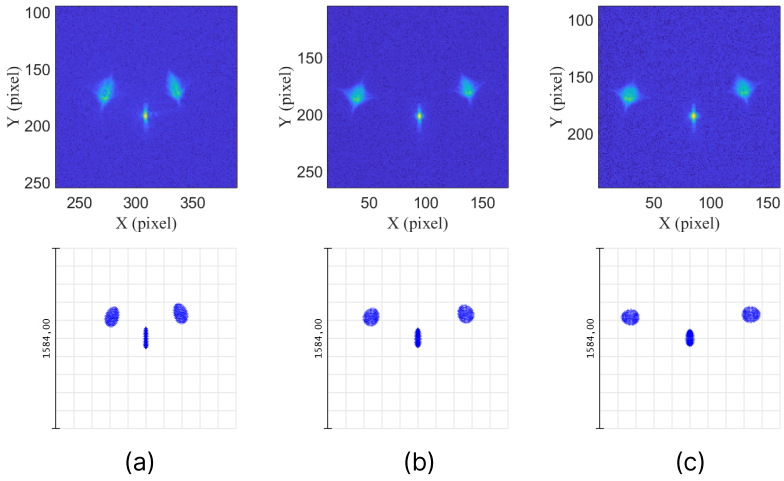

Figure 5.3: Images of the spots and their corresponding simulation with the camera at about $249.3\ mm$ from the M1 plate support (a) and moving the camera $0.5\ mm$ (b) and $1.0\ mm$ (c) closer to the mirror

The diameter of the laser beams used for the comparison is 8 mm.
The comparison between the simulated spot diagrams and the images taken by the camera proves the correct conic constant.
The central spot, corresponding to the central laser beam, has lower dimensions in the acquired images due to the fact that M1 was mounted inside its mechanical support, which has a smaller central aperture than the size of the beam used for the analysis.

5.1.2 Characterization of mirror M3

With a similar method as in the case of M1, mirror M3 has been characterized comparing the images taken with a camera and the simulation on Zemax.
In this case, the setup is different because the mirror is not positioned inside the telescope, but on a platform. As before, the three laser beams are reflected by the mirror to a camera on a linear motion stage. The experimental setup is schematically represented in Figure 5.4.

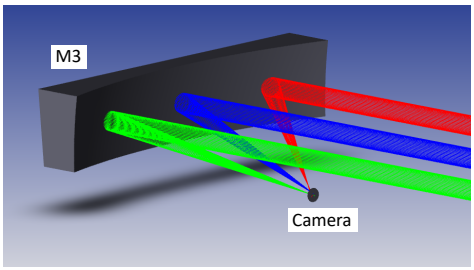

Figure 5.4: Scheme of the experimental setup used to characterize M3

The analysis has been performed considering a reference position located at 108.13 mm from the vertex of M3. The spots in this position are shown in Figure 5.5.

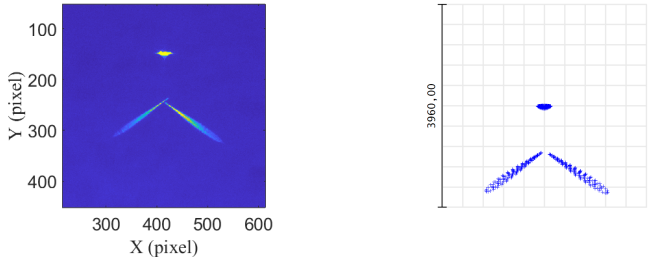

Figure 5.5: Acquired image and the simulation on Zemax of the spots on the reference position

Then, the camera has been moved closer and farther of $0.5\ mm$, $1.0\ mm$ and $1.5\ mm$ from the mirror to acquire more images. The results and their simulation are shown in Figure 5.6 and Figure 5.7.

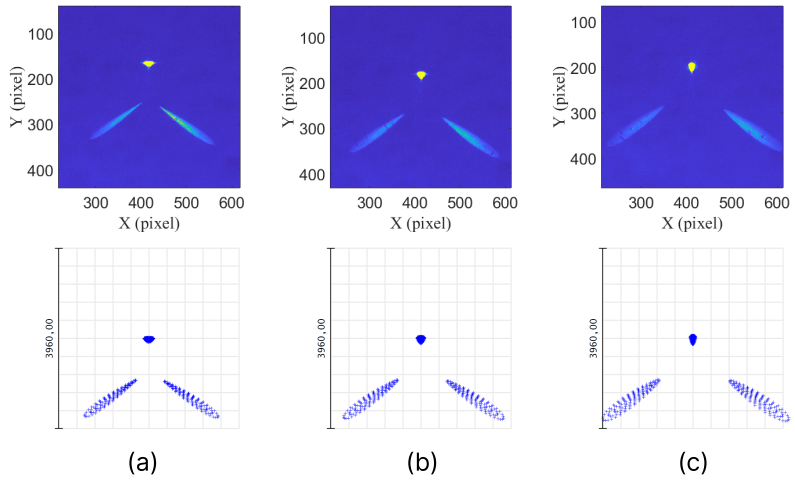

Figure 5.6: Images of the spots and their corresponding simulation with the camera at $0.5\ mm$ (a), at $1.0\ mm$ (b) and at $1.5\ mm$ (c) closer to the mirror from the reference position

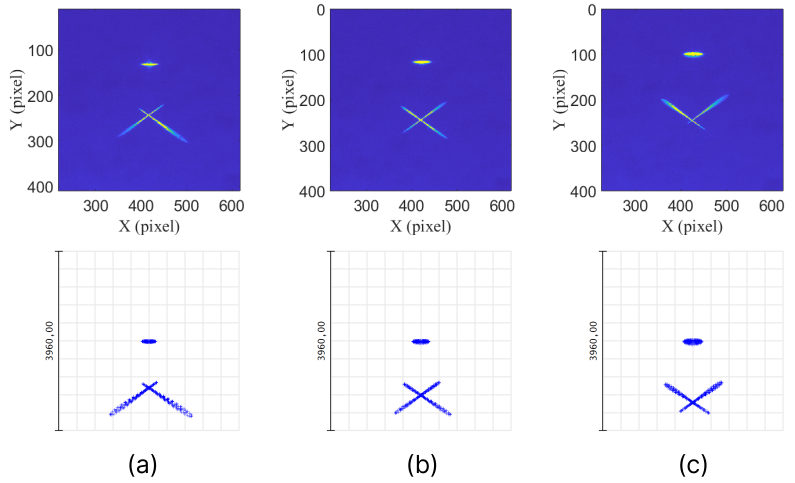

Figure 5.7: Images of the spots and their corresponding simulation with the camera at $0.5\ mm$ (a), at $1.0\ mm$ (b) and at $1.5\ mm$ (c) farther from the mirror from the reference position

The comparison of the spots proves that the mirror M3 has the correct conic constant.
In this analysis, the diameter of the laser beam is $10\ mm$.

5.2 Schmidt-Pechan prisms

The two Schmidt-Pechan prisms are the optical elements which perform the rotation of the FoV. In particular, the rotation of 90 degrees of the FoV is realized with a tilt of the prisms of 45 degrees. To understand better the rotation of the image, a prism can be compared to an axis of rotation. It is clear that a coming beam will be shifted on the other side of the axis of rotation keeping the same relative distance with the axis.

5.2.1 The alignment of the prisms

In order to have an inclination of the prisms of 45 degrees with respect to the HYPSOS base, a 3D printed support has been realized. This configuration provides a 90 degrees rotation of the image. The support is shown in Figure 5.8.

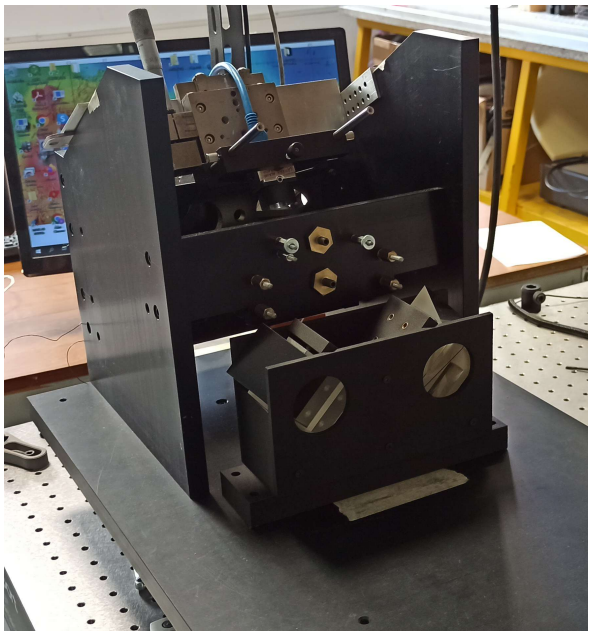

Figure 5.8: The two Schmidt-Pechan prisms inside their support

To verify the correct inclination of the prisms, a chessboard target has been placed in the focal point of the collimator lens in the second path. Then, using a camera, images of the chessboard have been analyzed to measure the orientation of the lines in the target lines, with and without the prisms inserted along the optical path. A schematic representation of the setup is shown in Figure 5.9.

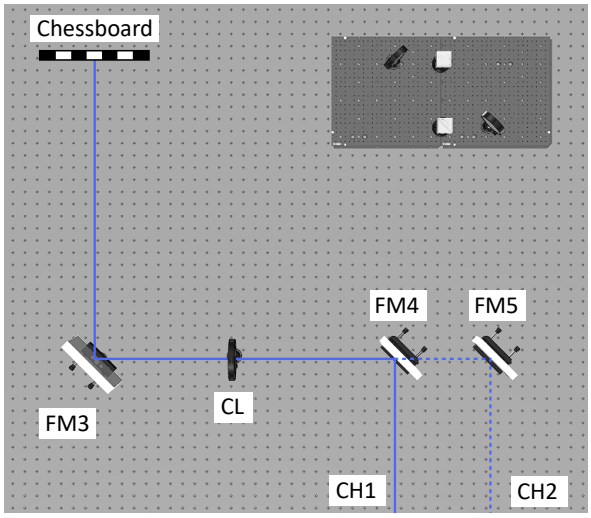

Figure 5.9: The experimental setup for the acquisition of the chessboard

From the images of the chessboard taken without the prisms, the tilt α of the target has been measured. Then, studying the images taken with the prisms, the tilt β is measured. Since introducing these prisms on the optical path provides a rotation of the image around the prism axis of an angle that is twice the prism inclination θ, the latter can be calculated as described in Equation 5.1.

$$\theta = \frac{\alpha - \beta}{2} \tag{5.1}$$

The rotation performed by the prisms is shown in Figure 5.10.

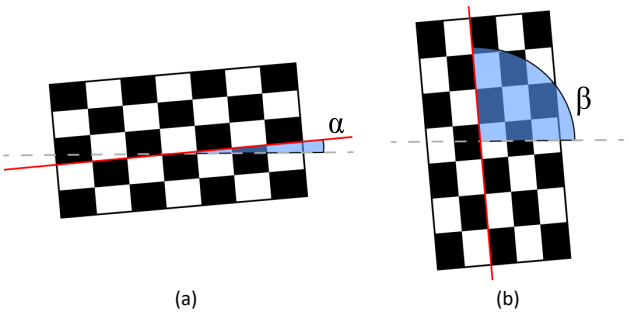

Figure 5.10: The chessboard seen by the camera with the prisms (b) and without (a)

The measurement of the chessboard tilt has been performed using a MATLAB tool for stereo calibration. The tool finds the position x and y of the corners of the chessboard. Then, it is possible

to calculate the line that fit the corners of the same row or column. The mean of the angular coefficient of the lines provides the inclination of the target. This analysis leads to the measurement of the chessboard's tilt with and without the prisms. Figure 5.11 and Figure 5.12 show the images acquired without and with the prisms.

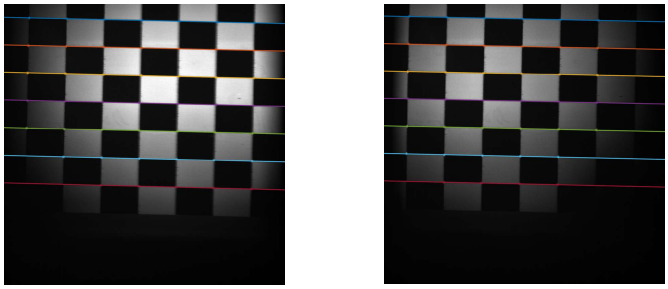

(a) (b)

Figure 5.11: The chessboard seen by the camera without the prisms: CH1 (a) and CH2 (b)

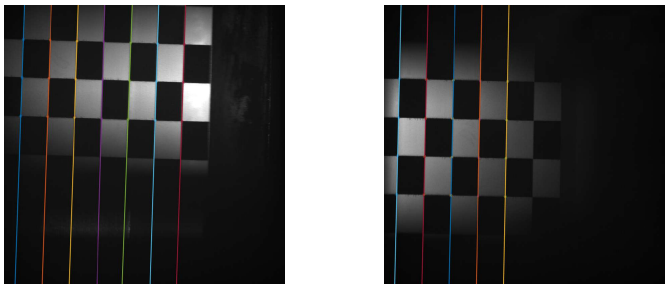

(a) (b)

Figure 5.12: The chessboard seen by the camera with the prisms: CH1 (a) and CH2 (b)

The angles of the two prisms have been corrected to minimize the error with the nominal configuration. Table 5.1 shows the obtained chessboard and prisms inclinations.

Prism	α $[deg]$	β $[deg]$	**Prism tilt** $[deg]$	**Error** $[deg]$	**Percent error** $\%$
CH1 prism	-1.322	88.166	44.744	0.256	0.6
CH2 prism	-1.176	88.797	44.986	0.014	0.03

Table 5.1: Tilt of the chessboard with and without the prisms

5.3 TMA alignment

The main procedure used to align every HYPSOS TMA component consists in the assembly of the optical elements, following the mechanical drawing, and in the comparison of the reflected spots with the Zemax simulation. Every mirror, except the folding mirror, lays inside a metal box with three apertures to let the light reach the surface of the mirror and to be reflected by the optical element, as shown in Figure 5.13. The boxes have internal size larger than the mirror's dimensions to let metallic plate springs to be placed between the mirror and the internal surfaces of the box. This configuration pushes the mirror to a central position. Precise movements are performed using a set of screw on the sides to adjust the mirror's position. On the back side of the box, four threaded rods allow to correct tilts and a ball point screw allows to correct the position along z-axis. In addition, for M1 and M3, four springs, placed near the corners of every box, reduce the weight on the threaded rods. After positioning every mirror, the reflected spots created by the laser from the first path have been analyzed and compared with Zemax simulations. The three laser beams have been modeled in the software to recreate the same conditions and to predict the position of the spots. Then, the analyzed mirror has been tilted until obtaining similar results to the simulation.

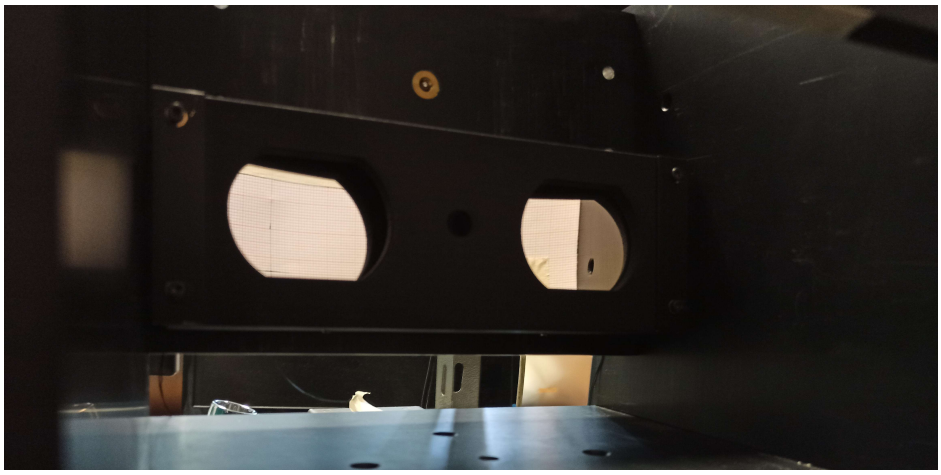

Figure 5.13: M1 inside its box during the alignment phase

5.3.1 M1 alignment

The mirror M1 is the first optical element that has been assembled to align the telescope. After laying the mirror inside the box and correcting its position through the screws, it was possible to assembly the box inside HYPSOS main structure.
Considering the optical disposition of the mirror, the position of M1 box has been calculated respect to the HYPSOS main structure. Resulting that, the box must be at 3 mm from the metallic plate which the box is attached to. According to this configuration, the laser beams are reflected to the surface where M2 mirror is supposed to be located. From the 3D model of HYPSOS in Inventor the position of this surface respect to M1 position has been estimated. Then, Zemax simulated the position of the spots on HYPSOS structure and their relative distances, as shown in Figure 5.14. The mirror has been tilted to obtain similar results to the ones simulated on Zemax. In order, to increase the precision of the alignment, a millimeter paper has been placed on the surface where the spots are displayed. The results are shown in the Table 5.2.

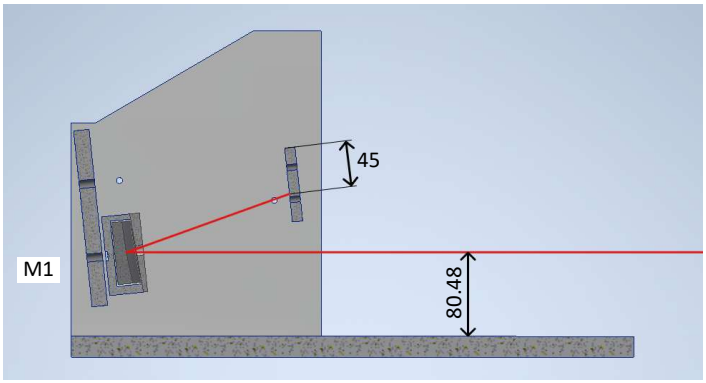

Figure 5.14: Representation of the alignment of M1

Spot	Relative distance to the central spot [Zemax]	Relative distance to the central spot [obtained]
CH1	16.4	16.5
CH2	15.9	15.5

Table 5.2: Results of the alignment of M1 (results are in mm)

5.3.2 M2 alignment

With a similar method used for the alignment of the mirror M1, M2 has been inserted in its box and assembled inside HYPSOS structure.
The box is located at 3 mm from the metallic plate where it is attached to. M2 position allows to collect the light from M1 and to reflect it to M3. During this phase, M2 reflects the laser beam to the plate where M3 is supposed to be located, as shown in the Figure 5.15. The results of the alignment have been compared with Zemax and are reported in the Table 5.3.

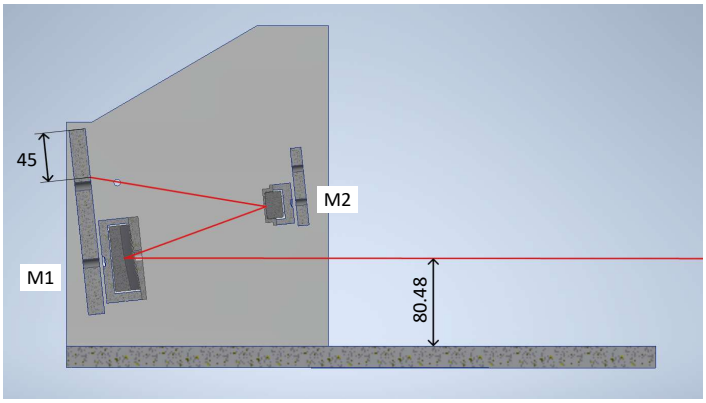

Figure 5.15: Representation of the alignment of M2

Spot	Relative distance to the central spot [Zemax]	Relative distance to the central spot [obtained]
CH1	35.5	36
CH2	34.5	34

Table 5.3: Results of the alignment of M2 (results are in mm)

5.3.3 M3 alignment

The procedure for the alignment of M3 is almost equal to the procedure performed for M1. The position of M3 is above M1 with identical distance between the box and the HYPSOS main structure as M1 box. M3 collects the light from M2 and reflects it to the support where the folding mirror is supposed to be placed as shown in Figure 5.16. The mirror is tilted to have the reflected spots compatible with the ones simulated on Zemax. Results are shown in the Table 5.4.

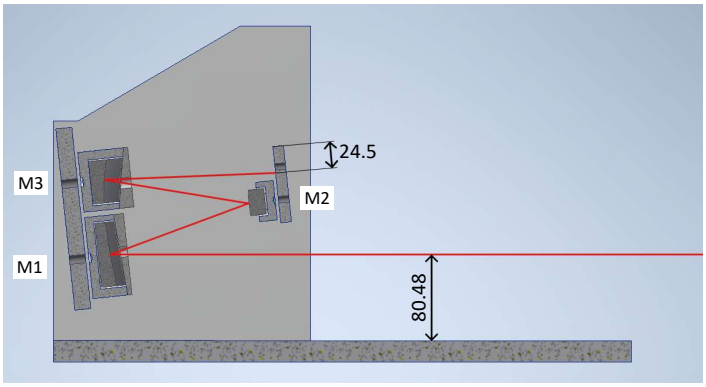

Figure 5.16: Representation of the alignment of M3

Spot	Relative distance to the central spot [Zemax]	Relative distance to the central spot [obtained]
CH1	0.77	0.75
CH2	0.75	0.75

Table 5.4: Results of the alignment of M3 (results are in mm)

5.3.4 FM alignment

The folding mirror is the only mirror which has a different support. The mirror is glued to the support and not placed inside of a box as in the case of the other mirrors.
The folding mirror is the last mirror before the spectrometer. In this case, the laser beams are not reflected to a surface of HYPSOS structure. For this reason, a millimeter paper has been placed on a precise position along the direction of the beams to project the spots on this surface, as shown in Figure 5.17. Like in the other cases, the mirror has been tilted until the spots reach the predicted position obtained on Zemax, as shown in the Table 5.5.

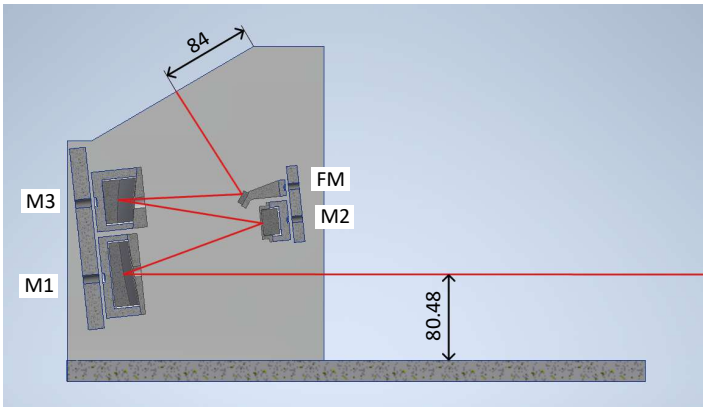

Figure 5.17: Representation of the alignment of FM

Spot	Relative distance to the central spot [Zemax]	Relative distance to the central spot [obtained]
CH1	15.6	16
CH2	15.2	15

Table 5.5: Results of the alignment of FM (results are in mm)

5.3.5 Precise alignment of the TMA

The method described to align the telescope does not provide a high accuracy. The spot position in the millimeter paper has an estimated error around $0.5\ mm$ and no information about the shape and the FWHM of the spots. To solve the problem, a camera has been placed on the telescope's focal plane, as shown in Figure 5.18.

The images acquired by the camera have been analyzed by means of a MATLAB script while two laser beams provided by the first path entered the two HYPSOS channels. In particular, the relative distance between the two spots and the FWHM are calculated. For this purpose, two images are acquired with one of the channels covered. This allows to have a single spot in every acquisition and to know which channel the spot corresponds to. Then, centroids are calculated with a 3D gaussian fit. From this information, the relative distances between the spots along x-axis and y-axis are estimated. The FWHM of both the spots are obtained by the same fit.

From the optical design, the two spots must be separated by about $60\ \mu m$ and with a FWHM of $19.88\ \mu m$ considering a laser beam diameter of $8\ mm$. The result is obtained with the merit function of Zemax. This feature allows to set a target configuration from initial conditions and specifying which degrees of freedom are involved in the simulation. For the TMA alignment, the initial condition are the mirrors in the nominal configuration, as described in the optical design, while the degrees of freedom are the tilts around x and y axes of M1 and M3. The target of the function is the obtained relative distances of the spots in the focal plane. Running the simulation, the software calculates the tilts from the nominal configuration to the obtained one. Then, applying the same calculated tilts but with the opposite direction to the mirrors of HYPSOS, the correct configuration is achieved.

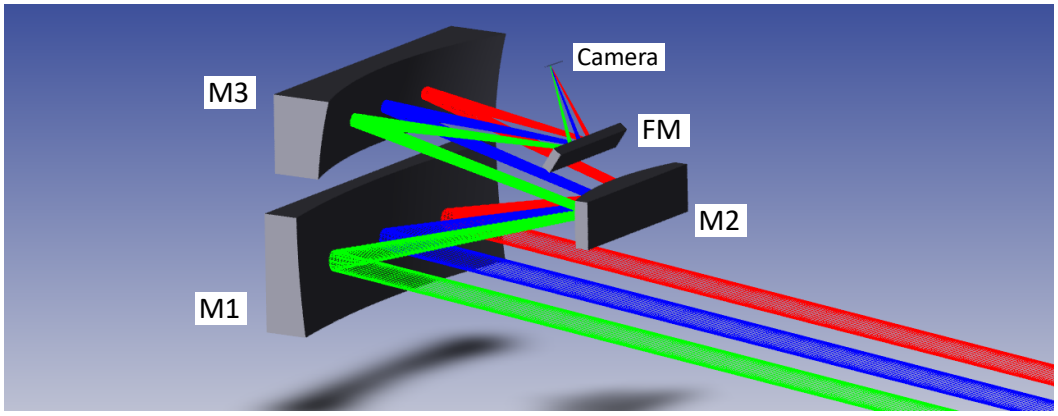

Figure 5.18: HYPSOS telescope in Zemax

During this analysis, it has been chosen to leave the mirrors M2 and FM in the simulation in their nominal position. The reason is that the two mirrors are placed using a calibrated metal plate to keep the correct distance between the supports of the mirrors and HYPSOS structure. Tilts around z-axis of the mirrors are not taken in account because the supports do not allow this correction.
The obtained outcome by the alignment using the merit function is much closer to the expected result than using only the millimeter paper. The results are shown in the Table 5.6 and in Figure 5.19.

Results	Relative distance between the lateral spots $[\mu m]$	FWHM CH1 $[\mu m]$	FWHM CH2 $[\mu m]$
Obtained	56.6	20.72	20.02
Expected	60	19.88	19.88

Table 5.6: Results from the alignment with the Zemax merit function ($8\ mm$ laser beam diameter)

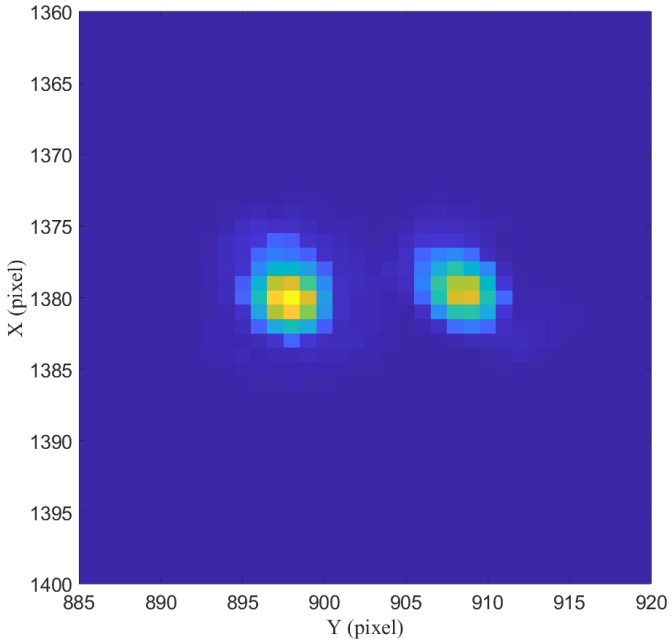

Figure 5.19: Image of the spots with the camera on the telescope's focal plane

5.3.6 MTF analysis

The Modulation Transfer Function is a method to estimate the resolution and contrast of an optical system: resolution is the ability of an optical system to separate object details; the contrast is the capability of and optical system to discriminate differences in signal intensities, from a maximum to a minimum.
Two methods to calculate the MTF are described in this section. The first one consists in the acquisition of the 1951 USAF target, while the second one is the Slanted Edge method. An image of the USAF target acquired by HYPSOS telescope is shown in Figure 5.20.

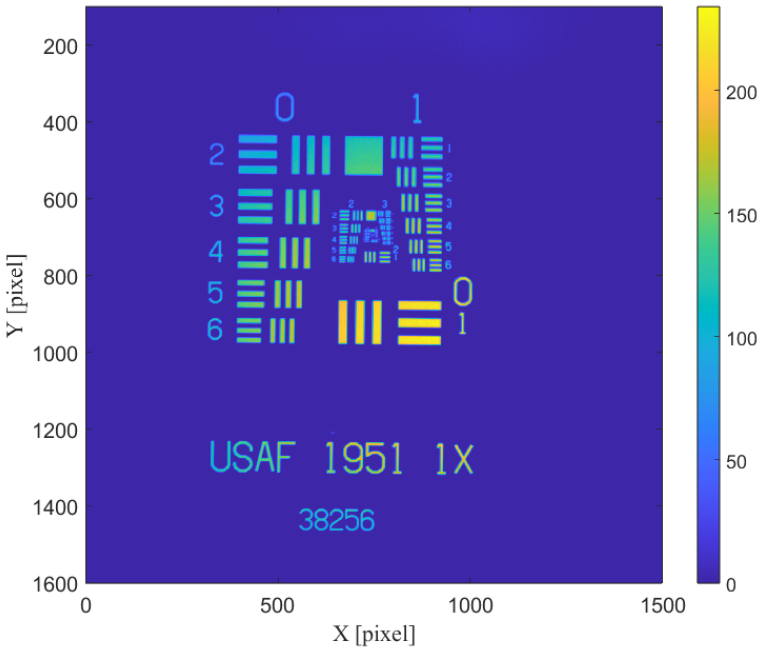

Figure 5.20: The 1951 USAF target acquired by HYPSOS telescope

The used setup is the same in both cases. The illuminated target is placed in the focal point of the collimation lens in the second path. The collimated light feeds the TMA telescope using a single channel at a time. Then, the image is acquired by a camera located on the focal plane of the telescope and it is analyzed with MATLAB scripts.
The images acquired with the USAF target are studied analyzing the elements that can be distinguished from each other. Elements with horizontal lines are studied along the vertical direction through a sinusoidal fit shown in Equation 5.2 and in Figure 5.21.

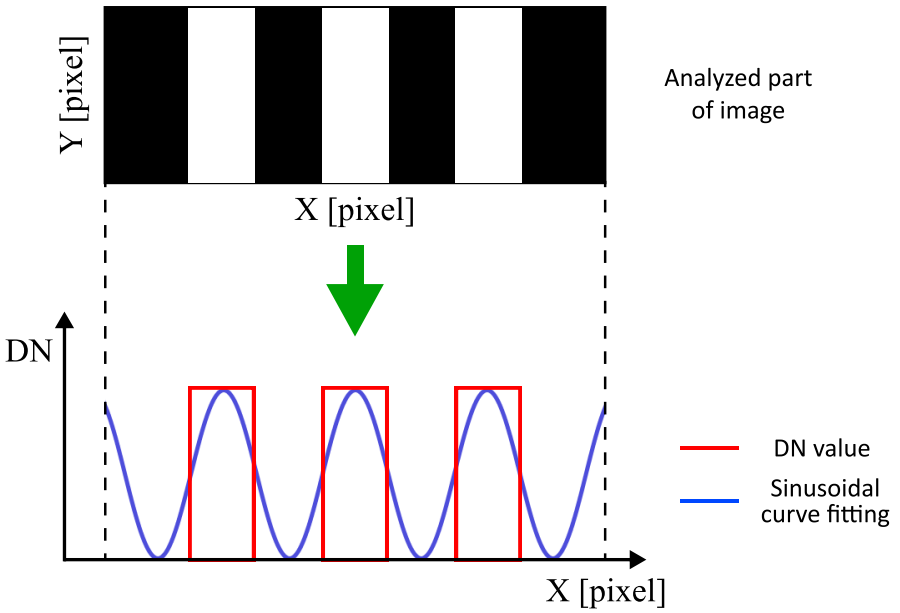

Figure 5.21: Graphical representation of the sinusoidal fit

$$f(x) = A\sin(b \cdot x + c) + d \tag{5.2}$$

The parameters of the fit are used to calculate the Contrast Transfer Function (CTF) as shown in the Equation 5.3:

$$CTF = \frac{\max - \min}{\max + \min} = \frac{A}{d} \tag{5.3}$$

where the max and min are respectively the maximum and minimum values of the sinusoidal function that correctly fit the DN values. Equation 5.3 shows that the CTF value is nominally equal to the fraction between the parameters of the fit A and d. The value obtained is relative to an element in the USAF target which corresponds to a precise value of spatial frequency. Studying many elements and groups in the USAF target, the CTF as a function of the image spatial frequency is acquired. From the CTF, the MTF is approximately calculated as shown in the Equation 5.4.

$$MTF = \frac{\pi}{4} CTF \tag{5.4}$$

The results of this measurements are shown in Figure 5.22.

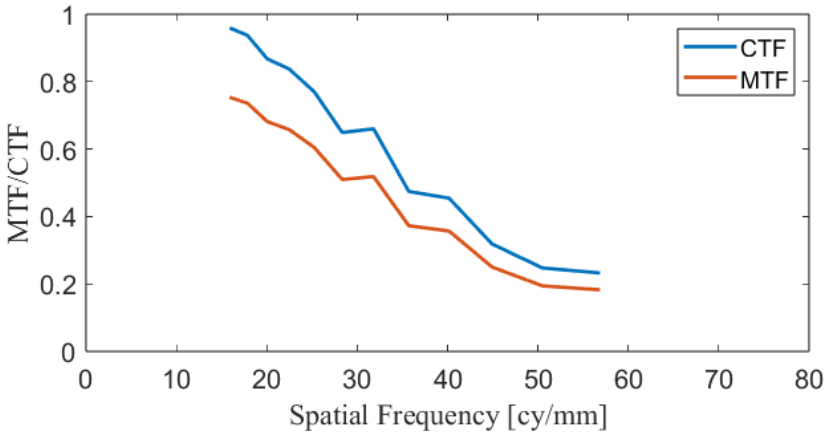

Figure 5.22: The obtained MTF and CTF using a sinusoidal fit

The second method to calculate the MTF, the Slanted Edge method, requires the acquisition of a knife edge. For this purpose, the 1951 USAF target can still be used because its edges are sharp and calibrated. The analysis provides more accurate result when the edge has a tilt between 4 and 6 degrees. The center of every pixel is projected on a line perpendicular to the edge; this lines is the abscissa axis of a plot in which the ordinate axis is the DN value of the signal collected on each pixel. The obtained graphic is the projected Edge Spread Function (ESF), as shown in Figure 5.23.

The following step to calculate the MTF is to plot the Line Spread Function (LSF), which is the ESF derivative. During this analysis, a smoothing spline function is used to fit the ESF. Then, the MTF is calculated from the Fourier Transform of the LSF. All the plots are shown in Figure 5.24.

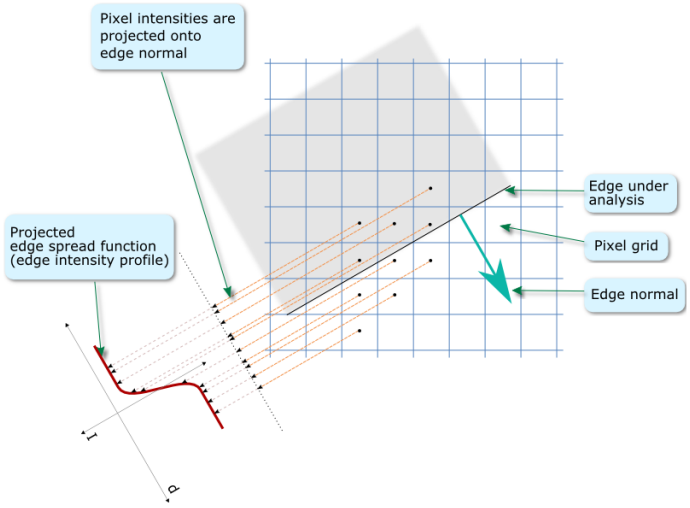

Figure 5.23: Representation of the projected Edge Spread Function

The comparison between the two methods is shown in Figure 5.25.

The two methods show similar results, but the Slanted Edge method is very sensitive to imperfections on the edge and on the surface of the target. In order to improve the quality of the analysis a flat field is required to normalize the image of the target. Both the resulting MTF are lower than the expected one.

5.4 Conclusions

The characterization analysis proved that the mirrors have features compatible with the ones required by the optical design.

Concerning the alignment of the prisms, the two prisms have been correctly tilted, but during the procedure it has been noticed issues on their support. This last one is not rigid and it bends screwing the screws which keep the prism in a fixed position. The issue can be solved considering another design of the support and using a different material.

From the telescope alignment, the obtained results are similar to the expected ones when the TMA is studied with the laser beams, but the MTF shows that the alignment has to be improved to match the features from the design. In particular, the procedure of alignment has been repeated different times during all the study of HYPSOS, because the TMA is very sensitive to vibration and thermal expansion.

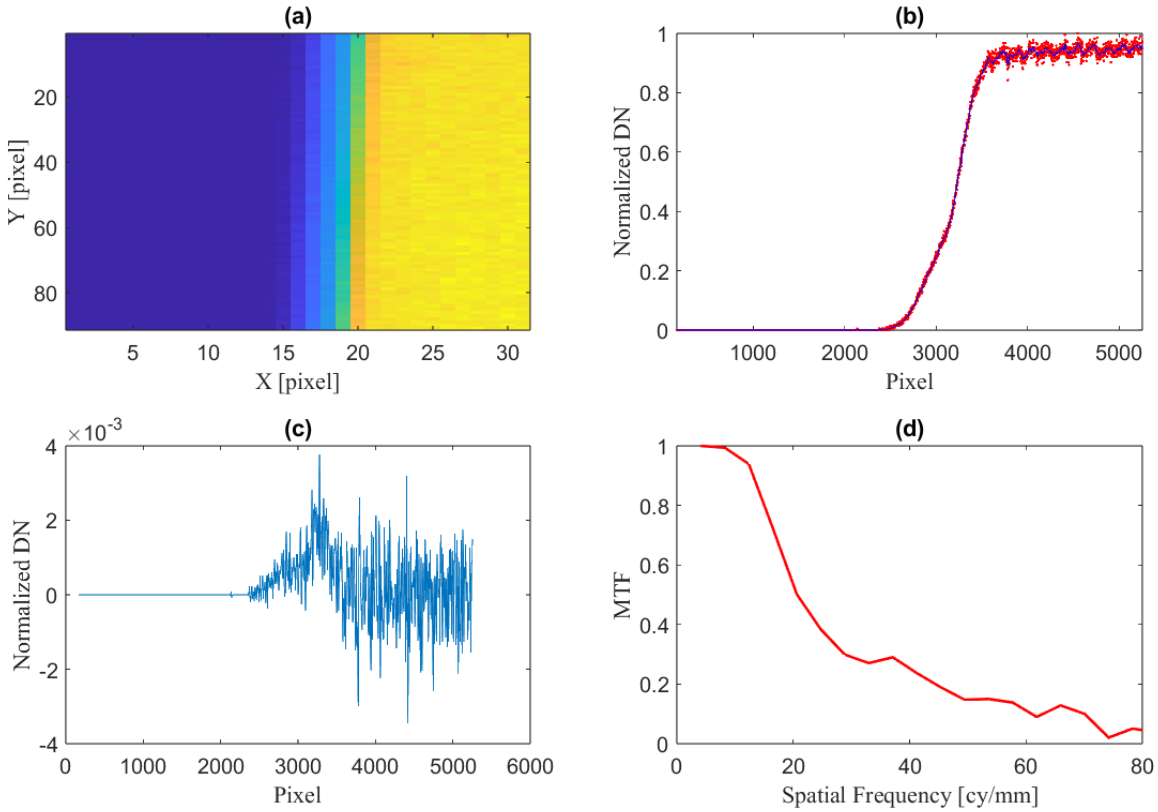

Figure 5.24: The results from the Slanted Edge method: the studied portion of image (a), the projected Edge Spread Function (b), the Line Spread Function (c) and the MTF (d)

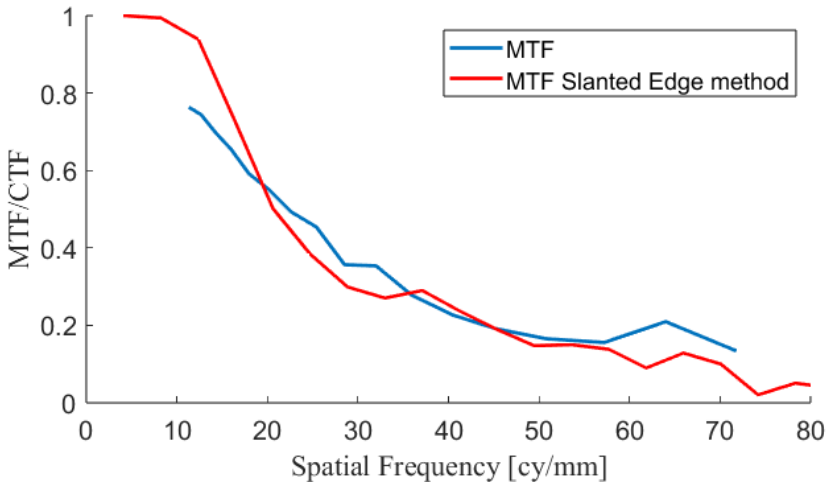

Figure 5.25: The comparison between the MTF calculated with a sinusoidal fit and with the Slanted Edge method

6

Assembly of the spectrometer on the telescope

During the last phases of analysis of HYPSOS, the spectrometer has been assembled on the telescope to obtain an initial study on the complete instrument. The spectrometer has been assembled to the telescope through two 3D printed lateral supports, as shown in Figure 6.1 and Figure 6.2.

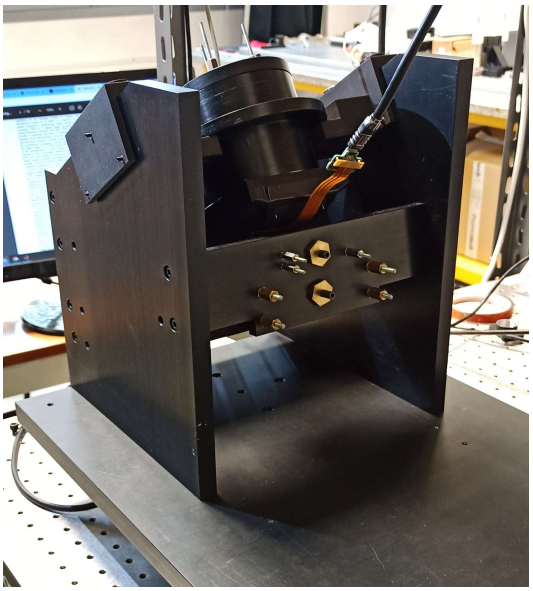

Figure 6.1: The spectrometer assembled on HYPSOS telescope

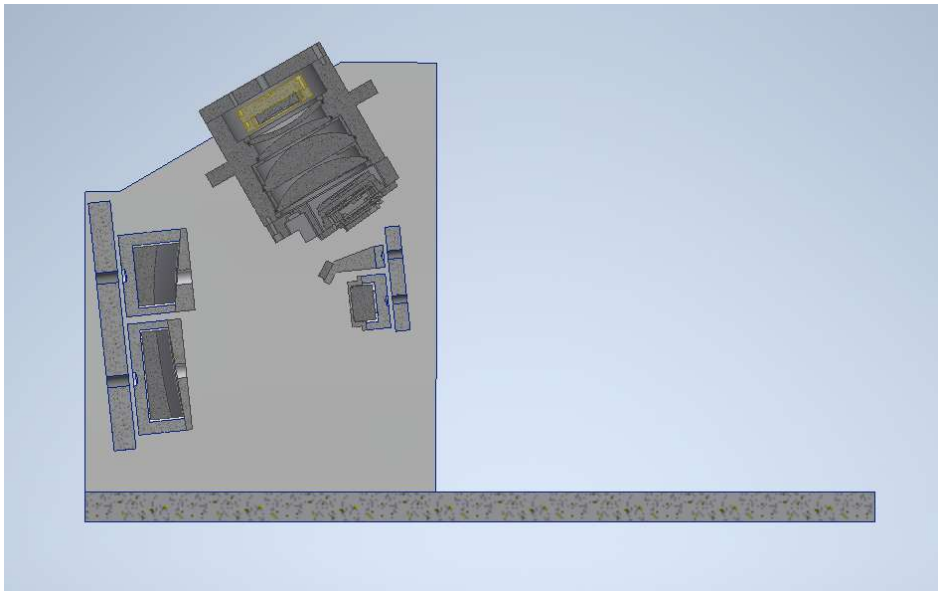

Figure 6.2: 3D model of the spectrometer on the telescope

At this stage it has been noticed that the weight of the spectrometer causes the bending of the two supports. This means that the slit aperture of the spectrometer may be not on the focal plane of the telescope. During this initial phase, this issue has been not considered. For this test, the pinhole slit was used as aperture of the spectrometer to provide a better characterization.

6.1 Acquisition of a spectral lamp

After the spectrometer has been assembled on the telescope, a spectral lamp has been placed in front of the aperture of CH2. This temporary configuration allowed to acquire a first spectrum with the system almost complete. In this case, the incoming light is not collimated to illuminate more pinholes. Otherwise, a collimated light would focus on the telescope's focal plane feeding a single pinhole. The adoption of a not collimated light required to cover the other channel to avoid crosstalking and straylight inside the telescope.
The acquisition of the image is different from the one obtained with only the spectrometer. In this configuration, the peculiar illumination path of HYPSOS is achieved, which means that rays enter the spectrometer with the angle described in the optical design.

The spectrum of a He lamp has been acquired and studied. The spectrum obtained by the assembly is shown in Figure 6.3.

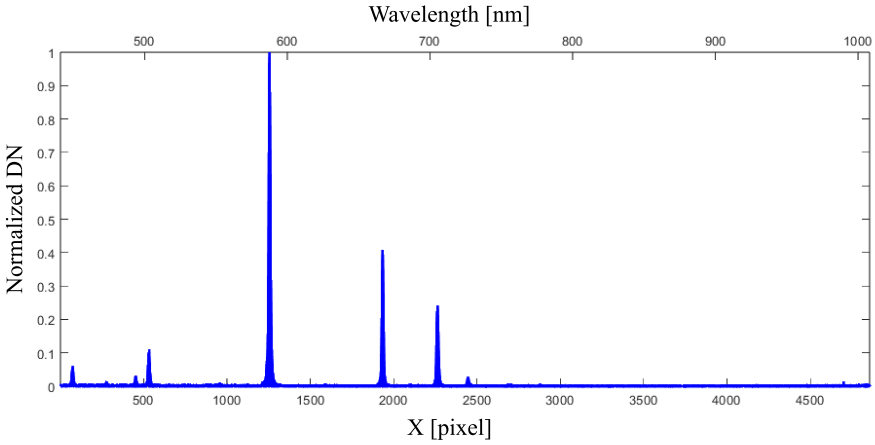

Figure 6.3: The spectrum obtained by HYPSOS of the HeI spectral lamp

The spot analysis has been performed on the spot corresponding to the wavelength 587.58 nm. Using the same methods described to calculate the FWHM, the spot has been characterized, as shown in Figure 6.4. The spatial FWHM is about 21 μm, which corresponds to the pinhole aperture of 22 μm. Along the spectral dimension, the FWHM is of 13 pixel, corresponding to a spectral width of 1.5 nm. On the side of the spot a ghost is visible.

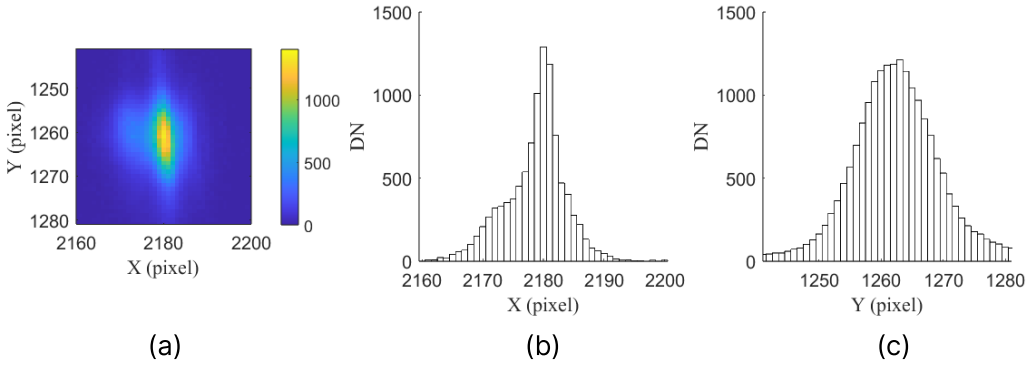

Figure 6.4: Image of the spot corresponding to the wavelength 587.58 nm of the HeI spectral lamp (a) with the FWHM analysis along the spatial dimension (b) and along the spectral dimension (c) [pixel size = 5.5 μm]

7 Conclusions

The alignment and characterization of HYPSOS consisted in the study of the spectrometer and the telescope. In order to obtain a complete characterization, an experimental setup has been designed and created.

The analysis of the spectrometer showed results compatible with the performance foreseen by the optical design. In particular, the position and orientation of the lenses and the diffraction grating match with the design. This has been verified comparing the obtained results with the simulations. For the analysis, it has been primarily considered the focal length of the lens system and the spot positions generated by the diffraction grating. The main observed issue is the fact that the sensitive area of the detector does not match completely with the focal plane of the spectrometer. Another observed problem is the presence of straylight on the detector, but it has been adequately resolved with a temporary cardboard mask and black duct tape.

Concerning the telescope, the characterization of the mirrors proved that the conic constant of the mirrors are equal to the ones in the optical design. The Schmidt-Pechan prisms have been correctly tilted inside their supports with acceptable relative errors. Then, all the mirrors of the telescope have been assembled inside HYPSOS structure and correctly aligned analyzing the FWHM and the position of the spots created by the laser beams on the focal plane of the instrument. The quality of the telescope has been checked studying a 1951 USAF target and calculating the MTF with two different methods. The result shows slightly lower performance than expected, but a relative good alignment.

Finally, the spectrometer has been assembled on the telescope for an initial test of the complete

instrument. The analysis of the FWHM of the spots created by a HeI spectral lamp showed compatible results with the expected ones.

References

[1] E. Hecht, "Optics - fifth edition," 2017.

[2] D. Meschede, "Optics, light and lasers," 2007.

[3] M. W. Justin Peatross, "Physics of light and optics," 2014.

[4] G. Naletto, L. Agostini, F. Brotto, G. Cremonese, M. Faccioni, L. Lessio, C. Re, M. Tordi, C. Bettanini, F. Capaccioni, M. T. Capria, S. Debei, E. Giovine, L. Marinangeli, F. Mattioli, M. Pertile, A. Petrella, G. Salemi, A. C. Tangari, and M. Zusi, "Laboratory characterization of hypsos, a novel 4d remote sensing instrument," 2021.

[5] G. Naletto, L. Agostini, G. Cremonese, E. Desirò, I. Dorgnach, C. Doria, M. Faccioni, R. L. Grassa, F. Lazzarotto, L. Lessio, A. Meneguzzo, C. Re, M. Tordi, C. Bettanini, F. Capaccioni, S. Debei, E. Giovine, L. Marinangeli, F. Mattioli, M. T. Melis, P. Palumbo, M. Pertile, A. Petrella, A. C. Tangari, and M. Zusi, "In-lab characterization of hypsos, a novel stereo hyperspectral observing system: first results," 2022.

[6] F. Mattioli, S. Cibella, R. Leoni, S. Orsini, A. D. Lellis, S. Selci, E. D. Angelis, R. Rispoli, A. Mura, and A. Milillo, "A nanotechnology application for low energy neutral atom detection with high angular resolution for the bepicolombo mission to mercury," *ScienceDirect*, 2011.

[7] "Theory and measurement of the modulation transfer function (mtf)," *Image Science Ltd*, 2015.

[8] T. Li, H. Feng, Z. Xu, X. Li, Z. Cen, and Q. Li, "Comparison of different analytical edge spread function models for mtf calculation using curve-fitting," 2009.

Acknowledgments

I would like to express my gratitude to Prof. Giampiero Naletto for giving me the opportunity to take part in this innovative project and for the support and professional guidance through these months. I am also thankful to Livio Agostini and Andrea Meneguzzo, my co-supervisors, whom I worked with on the project, for their help during the activities in the laboratory. I would like to mention also Prof. Alain Jody Corso and everyone I met in the Luxor laboratories for their useful advices. In these years at the University I had the pleasure to work with Alexandru Andrei Avram, Elisa Borgato, Elisabetta Dolejsi, Francesco Fontanot, Edoardo Ghinatti, Stefano Giaretta e Stefano Grigio. I am grateful to them for making the many hours spent studying more enjoyable. Another major thanks to Olha, my girlfriend, who supported me during the activities for this thesis and finally, my family for the support through all these years of study.

A Scripts

A.1 Motorized linear stage script

```
import pyfirmata
import time

# Define Arduino port
board = pyfirmata.Arduino('/COM5')

it = pyfirmata.util.Iterator(board)
it.start()

# Pin definition
dirPin = board.get_pin('d:2:o') # Direction pin
stepPin = board.get_pin('d:3:o') # Step pin

# Switch pin definition
switch_1 = board.get_pin('d:11:i') # Servo side switch
switch_2 = board.get_pin('d:12:i') # Opposite servo side switch
```

```
# Initialization of the movement parameters
stepsPerRevolution = 200 # Number of step per revolution
halfPeriod = 20000/32
maxStepNum = 153600  # Maximum number of steps
microStep = 1

# Initial message
print()
print("######################")
print("#### MOTION STAGE ####")
print("######################")
print()

# Initial position input
savetxt = "save.txt"

with open(savetxt,"r") as readfile:
   start_pos = readfile.readline()

print("Initial position:")
print(start_pos)

# Definition of the Motion function
def spost_fun():
   stepPin.write(1)
   time.sleep(halfPeriod/microStep*10**(-6))
   stepPin.write(0)
   time.sleep(halfPeriod/microStep*10**(-6))

# Definition of the Home function
def home_fun():
   # The stage activates the switch
   dirPin.write(0)
   while switch_1.read() == 0:
      spost_fun()
   # The stage moves until the switch is not activate
```

```
   dirPin.write(1)
   while switch_1.read() == 1:
      spost_fun()

# Instruction messages
print()
print("Digit home to reset the position")
print("Digit end to terminate the execution of the program")

end_script = 0
position = float(start_pos)

while end_script != 1:

   # Input of the command
   print()
   input_cmd = input("Shift in mm: ")
   print()

   # Activation of the Home function
   if input_cmd == "home":
      home_fun()  # Activate the Home function
      position = 0 # Saving the Home position

      # Debug print
      print("Current position:")
      print(position)

   # Shift
   if input_cmd.replace('.','').lstrip('-+').isdigit():
      shift = float(input_cmd)
      i_shift = int(shift/0.5*200) # Calculate the number of the steps

      # Determination of the direction of movement
      if i_shift > 0:
         dirPin.write(1) # The stage moves farther from the servo
```

```
    if i_shift < 0:
        dirPin.write(0) # The stage moves closer to the servo

    # Shift
    step_count = 0 # Count of the number of performed steps
    if input_cmd != 0:
        for i in range(abs(i_shift)):                    # For cycle with the
            steps to performe
            if switch_1.read() == 0 and switch_2.read() == 0: # If a switch is
                activated
                spost_fun()                              # Moves the stage
                step_count = step_count + 1              # Counts the number of
                    performed steps

    # Waiting time after the movement
    time.sleep(1)

    # Calculation of the new position
    if switch_1.read() == 1:   # If switch_1 is activated
        print("The motion stage reached the limit")
        print()
        position = 0
        # Moves the stage until switch_1 is deactivated
        dirPin.write(1)
        while switch_1.read() == 1:
            spost_fun()
    elif switch_2.read() == 1: # If switch_2 is activated
        print("The motion stage reached the limit")
        print()
        position = 101
        # Moves the stage until switch_2 is deactivated
        dirPin.write(0)
        while switch_2.read() == 1:
            spost_fun()
    else:
        if i_shift > 0:
```

```
            position = position + (step_count*0.5/200) # Calculate the position
         if i_shift < 0:
            position = position - (step_count*0.5/200) # Calculate the position

      # Debug print
      print("Performed shift [mm]:")
      print(step_count*0.5/200)

      # Debug print
      print()
      print("Actual position [mm]:")
      print(position)

   # Terminate the script
   if input_cmd == "end":
      end_script = 1


# Save the new position in the external file
print()
print("Final position [mm]:")
print(position)
with open(savetxt, "w+") as outputfile:
   outputfile.write(str(position))
```